

## Chapter 3

### X-Ray Diffraction

Diffraction is a phenomenon with which we are all familiar, if only as the cause of the rainbow on the surface of a compact disc, or on a puddle of water with a film of oil on top, or from the wing of a butterfly. These effects are dependent on the properties of light: wavelength, amplitude, and phase. For light in the optical range, we experience a change in wavelength as a change in color; a change in amplitude, we experience as a change in brightness; we cannot, however, directly experience a change in phase. We need to examine these phenomena as they apply to the interaction of X-rays and crystals. *The essential feature of the diffraction of waves of any wavelength is that the distance between scattering centers be about the same as the wavelength of the waves being scattered.* The dimensions of X-rays and the spacings between atoms in crystals meet these conditions, as von Laue and his group showed in 1912. The wavelength of X-rays and the structural spacings of crystals both have dimensions about  $10^{-8}$  cm ( $10^{-8}$  cm = 1 Å). In brief, this chapter develops the concept that X-rays are scattered by the electrons around the nuclei of the atoms composing a unit cell. This scattering is modified in three ways: (1) by the way in which the electrons of a particular atom are distributed within the field of influence of that atom; (2) by the thermal vibrations that tend to blur the atoms as scattering centers as temperature increases; and (3) by the way atoms are arranged within the unit cell. Each scattering center contributes a diffracted beam that can be represented by a vector. Atoms, unit cells, or crystallites (very small crystals) can be treated as

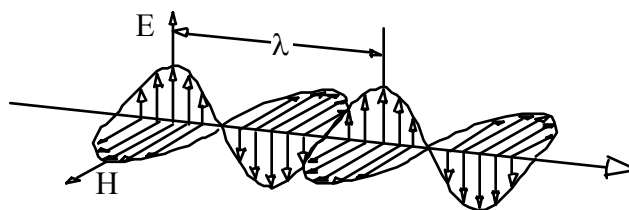


Fig. 3.1. A single, polarized ray of the X-radiation part of the electromagnetic spectrum. E is a vector representing the electrical field, and H is a vector representing the magnetic field. Wavelengths in this region of the spectrum range from 0.5 to 10 Å.

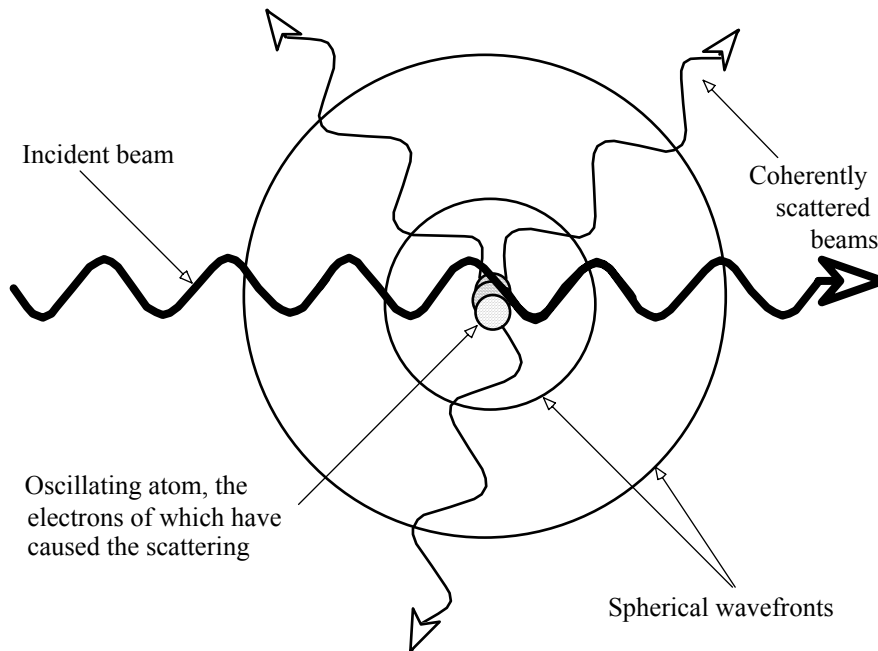


Fig. 3.2. An atom oscillating about its lattice point in the crystal structure behaving like a point source for radiation scattered spherically (like an isometric optical indicatrix).

scattering centers. All the vectors from scattering centers within an optically coherent domain must be summed into a single vector, and then the vectors from each domain must be summed. This will bring us to a resultant, diffracted beam with a specific amplitude and phase, and we will see that we can calculate the intensity of this beam to compare it to our experimental results.

## SCATTERING

Like all electromagnetic radiation, we can characterize X-rays in terms of a single, polarized ray with an electric vector  $\mathbf{E}$  vibrating perpendicular to the direction of propagation in one plane and a magnetic vector  $\mathbf{H}$  vibrating perpendicular to both the direction of propagation and to that of the electric vector (Fig. 3.1).  $\mathbf{H}$  will be of little interest to us, but  $\mathbf{E}$  of an incident photon is the stimulator of scattering. As an incident ray encounters an electron, the electron vibrates in resonance with  $\mathbf{E}$  (i.e., it vibrates with the same frequency). Because the electron is a charged particle, and a vibrating charged particle is an emitter of electromagnetic radiation, the vibrating electron becomes a beacon absorbing a small amount of energy from the incident beam and reradiating it in all directions at the same wavelength as the incident beam (Fig. 3.2). This phenomenon is called *coherent scattering*. (*Incoherent scattering* is scattered radiation with a wavelength longer than that of the

incident or stimulating radiation. The term *scattering* in this text refers to coherent scattering. For more about incoherent scattering, see Fig. 2.4, p. 36 and the topic Compton scattering in Cullity, 1978 or Klug and Alexander, 1974.)

The electrons doing the scattering that interests us are held in orbits around nuclei. Because each electron scatters, the scattering power  $f$  of an atom increases with the number of electrons bound to that atom. The scattering power of an atom is somewhat less than the scattering power of a single electron multiplied by the number of electrons in the atom. The reason is that outgoing waves scattered by electrons in different parts of the same atom will be slightly out of phase with each other and some destructive interference results. These effects increase with scattering angle; so scattering efficiency of an atom declines as the Bragg angle  $\theta$  increases. However, for our purposes we can consider each atom in a unit cell as a point source of scattered radiation and ignore most of these other details. We will discuss phase and Bragg angle shortly.

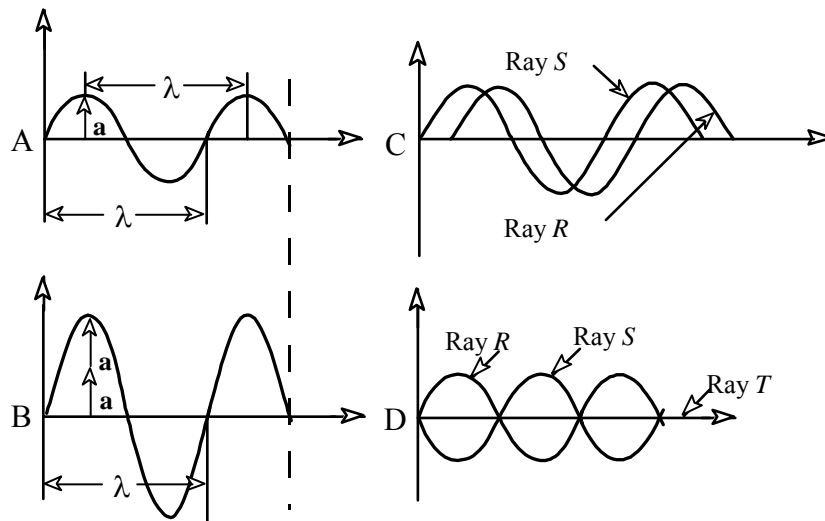


Fig. 3.3. Constructive and destructive interference. A. A sine wave representing an X-ray and showing amplitude  $a$ , a vector, and wavelength  $\lambda$ . B. Two rays exactly the same as the ray in A added together by constructive interference. Note that the same wavelength is maintained but the amplitude is doubled. The dashed line perpendicular to the rays in A and B is a wavefront, so called because it marks the same place in the progress of both rays. See the wavefronts in Fig. 3.4. C. Rays R and S are not in phase as were the two rays that added to make the ray in B. The resultant ray has an amplitude less than that in B. As the two rays approach being exactly out of phase the resultant amplitude will decrease to zero. D. Here rays R and S are exactly out of phase and the result is ray T or essentially no ray at all.

**INTERFERENCE**

Next, you need to understand what is meant by *constructive* and *destructive interference* of electromagnetic radiation. In short, there is constructive interference when two or more rays are in phase, and destructive interference when the rays are out of phase. In Fig. 3.3, A shows the wavelength  $\lambda$ , and that wavelength is the same from point to similar point. A line drawn perpendicular to the direction of propagation touches both rays in A and B at exactly the same state: at the point of zero amplitude. (Such a perpendicular line is called a *wavefront*.) Think of the amplitude of each ray at each increment of propagation as a vector (Fig. 3.3). In all cases, whether interference is constructive or destructive, the amplitude portion of the vectors add, like the **a** vectors in B, which represents the adding, or constructive interference, of two waves equal to the wave in A. C shows two rays, *R* and *S*, that are not in phase. Try putting a line perpendicular to their direction of propagation. Does it meet the criterion given for that shown in A and B? The amplitude vectors will add here also, but in some cases, one vector will be positive and the other negative, thus partially or completely canceling one another out reducing the amplitude to something less than that shown in B. Additional rays, also slightly out of phase with *R* and *S* would again reduce the amplitude and change the phase of the resultant ray, as would each additional ray that was out of phase. Now, in Fig. 3.3D, imagine that the amplitude vectors of rays *S* and *R* are added. Do you see that each would exactly cancel out the other resulting in ray *T*? This is completely destructive interference.

When two or more rays constructively interfere, a diffracted beam is produced, but to be useful there must be many mutually constructive rays. *A diffracted beam that we can observe and measure is a beam composed of an enormous number of constructively interfering rays, rays that are mutually reinforcing one another.* Now, what sort of condition will lead to such an observable beam?

***Scattering from a Row of Atoms***

Figure 3.4 shows how a diffracted beam can be formed as rays move through a row of regularly spaced atoms. Figure 3.4A shows wavefronts of the incident beam advancing parallel to a row of eight atoms, each of which, stimulated by the passing wavefront, becomes a beacon sending out waves of the same wavelength as the exciting radiation. Just like the single atom in Fig. 3.2, the scattering from the eight atoms is spherical and is represented here by concentric circles with radii of one, two, and three wavelengths. Any lining up of spherical wavefronts makes a mutually reinforced wave moving in the direction perpendicular to a tangent common to the spheres. The most obvious case of this is shown in Fig. 3.4B where wavefront *A* is the wavefront of a diffracted beam traveling straight ahead and parallel to the incident exciting

rays. This wavefront is a line tangent to the sphere one wavelength from each atom. Though this shows the simplest case, this particular diffracted beam is overlaid by the incident beam. Therefore, it cannot be observed. We can find other diffracted beams, however.

Figure 3.4C shows wavefronts for three diffracted beams. Imagine that the spherical wavefront from atom 8 has just begun to scatter so that it is a point rather than a sphere. A line from this point tangent to the spherical wavefront that has traveled one wavelength from atom 7 is tangential to the spherical wavefront that has traveled two wavelengths from atom 6, that has traveled three wavelengths from atom 5, and so on. This line makes wavefront  $B$ . Diffracted beam  $B'$  is traveling perpendicular to wavefront  $B$ . Do you see the patterns for the other diffracted beams? For example, notice that wavefront  $C$  is tangent to wavefronts from atoms 2, 4, 6, and 8 or every second atom. What is the pattern for wavefront  $D$  and its associated diffracted beam? Do you see that if the atoms were not evenly spaced or periodic there could be no constructive interference and, therefore, no diffraction?

The three wavefronts in Fig. 3.4C also show that diffraction occurs at specific angles, with no diffraction in the angular regions between diffracted beams; i.e., there is no diffraction effect between  $B'$  and  $C'$ . We will demonstrate later that the angles of  $B'$  and  $C'$  to the line of atoms are functions of the wavelength of the incident radiation and the spacings of the atoms (Bragg's law, p. 69). Perhaps you can see that from Fig. 3.4C.

Another way to look at Fig. 3.4A to see where diffracted beams are formed is to realize that anywhere two spherical wavefronts intersect, rays coincide and their amplitudes add; in other words, there is constructive interference. For example, at points  $a$ ,  $b$ , and  $c$  there is mutual reinforcing by spherical wavefronts from atoms 4 and 5. In addition, the third wavefronts from atoms 3 and 6 add to the amplitude at point  $b$ . These reinforcements make a diffracted beam, shown by the line drawn through  $a$ ,  $b$ , and  $c$ , traveling in the same direction as the incident beam.

Where the first wavefront from atom 5 (Fig. 3.4A) and the second wavefront from atom 4 intersect (point  $d$ ) and the second wavefront from 5 and the third from 4 intersect (point  $e$ ), a second diffracted beam is created. Whether we picture the diffracted beams as shown in Fig. 3.4A or as defined by the tangents as shown in Fig. 3.4C, there is a small, finite number of beams at discrete angular spacings. There is *not* an infinite number of diffracted beams.

Now, before we go on to visualize diffracted beams created by scattering from atoms in three dimensions, let us consider a row of atoms such as that shown in Fig. 3.4A, scattering not in two dimensions as shown, but in three dimensions. Picture the intersection above the plane of the paper of the first spherical wavefronts around atoms 4 and 5. Do you see that their intersection would describe a circle on a plane common to the beam defined by points  $a$ ,  $b$ , and  $c$  and this plane would be perpendicular to the plane of the paper? Likewise, the intersection of the second and third spherical wavefronts from

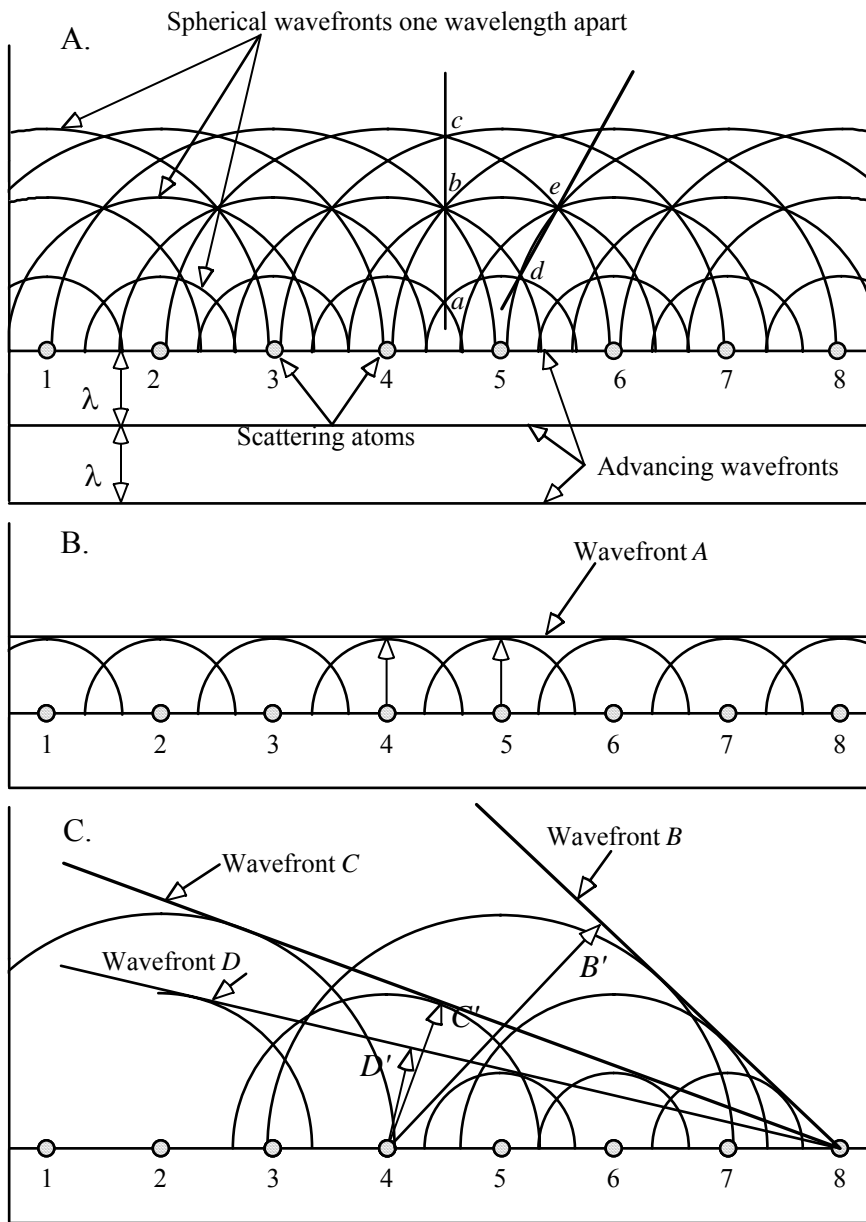


Fig. 3.4. Constructive interference of waves scattered by regularly spaced row of atoms. A. Wavefronts from each atom with reinforcing or constructive interference at points  $a$ ,  $b$ ,  $c$ ,  $d$  and  $e$ , e.g., wavefronts from atoms 4, 5, 6, and 7 contribute to the constructive interference at point  $e$ . B. A single wavefront of scattered, reinforcing waves. C. Reinforced scattering at other than the direction of the primary beam. Ray  $B'$ , for example, is perpendicular to wavefront  $B$ .

atoms 4 and 5 would trace circles on the same plane perpendicular to the paper. You should be able to picture a planar disk perpendicular to the paper that contains points  $a$ ,  $b$ , and  $c$ , and these points would be on concentric circles representing the intersecting spherical wavefronts of atoms 4 and 5.

Now that you have visualized this you hardly need Fig. 3.5, right?

If the sum of the diffracted beams represented by the line  $abc$  in two dimensions takes the shape of a disk in three dimensions, then what shape will be made by the diffracted beams represented by the line  $de$ ? Try to make it swing out of the plane of the paper from Fig. 3.4A toward you. Points  $d$  and  $e$  will each trace the intersections of spherical wavefronts. Concentrating on point  $e$  and the intersection of the second wavefront from atom 5 and the third from atom 4, can you see that as point  $e$  traces the intersection of these two spherical wavefronts it will trace a circle in a plane perpendicular to the paper? Point  $d$  also will trace a circle in a plane perpendicular to the paper, but it will be smaller. The sum of all diffracted beams connecting or defined by the two circles traced by  $d$  and  $e$  forms a cone, the axis of which is the row of atoms. This is represented in Fig. 3.5 and a cross-section of this figure containing lines  $abc$  and  $de$  would look like Fig. 3.4A.

From each pair of atoms in the row, a similar set of cones of diffracted beams will radiate. A cross-section of such a row would show whole sets of lines parallel to lines  $abc$  and  $de$ . For the circumstances shown in Fig. 3.5, a set of lines or rays would be in phase and therefore would mutually reinforce one another, resulting in a diffracted beam.

### ***Scattering from a Three-Dimensional Array of Atoms***

We are now ready to consider the manner in which a diffracted beam is formed as a result of scattering by the atoms of a three-dimensional crystal structure. To imagine a three-dimensional array of atoms, picture three rows of atoms like the one in Fig. 3.5. Figure 3.6 shows rows of atoms X, Y, and Z intersecting at right angles (as if the rows were a set of orthorhombic reference axes). In response to an incident beam, scattering from a single atom at the point of intersection is combined with scattering from an adjacent atom on each of the axes to form the three cones. The angle at which the cones open is related to the angle at which the incident beam strikes. A, B, and C of Fig. 3.6 show the cones opening at larger and larger angles as the incident beam approaches a Bragg angle (an angle at which constructive interference will occur). The cones represent diffracted beams. Where the cones intersect, the diffracted beams undergo additional constructive interference. In Fig. 3.6A the cones do not intersect. In B they just touch, so there would be three minor diffracted rays coming out of the quadrant enclosed by rows X, Y, and Z. In C they penetrate so that all three cones have one common line of intersection. The diffracted beams shown in Figs. 3.4 and 3.5 would have significantly less intensity than the diffracted beam of Fig. 3.6C. In addition, there will be a set of cones associated with each pair of atoms throughout the unit cell. All of this will result in whole families of parallel diffracted beams, the sum of which will produce a diffracted beam with intensity enough for us to observe. Do you see that this sort of diffracted beam will have greater intensities than those of a beam like  $de$  in Fig. 3.5

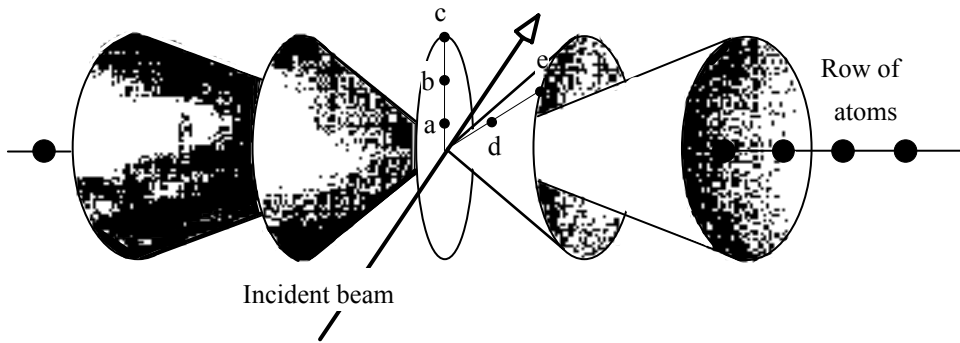


Fig. 3.5. Diffraction cones from the interaction of wavefronts from two adjacent atoms in a row of atoms. Points *a*, *b*, *c*, *d* and *e* are from Fig. 3.4.

because there are more atoms contributing to the scattering? The diffracted beam in Fig. 3.6C. can be described in terms of direction cosines. For this and for a more rigorous development of these steps, see Buerger (1942, pp. 29-43).

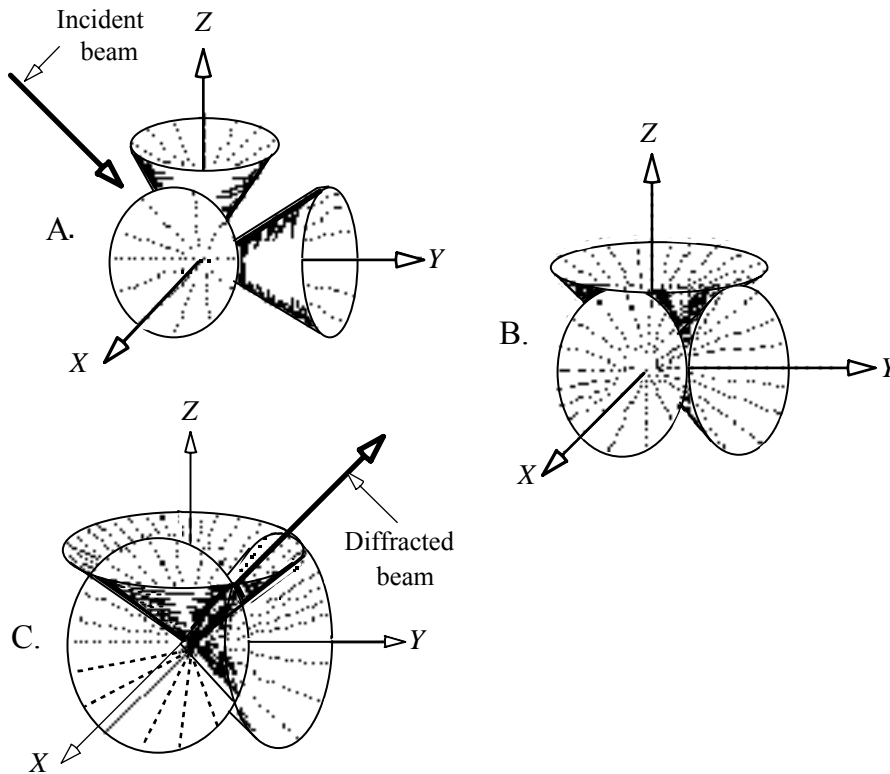


Fig. 3.6. Change in angle of cones of diffraction with change in the direction of incident beam until at a Bragg angle a reinforced diffracted beam is formed as in C.

**Bragg's Law**

Using a diffractometer to study clay minerals, we seldom deal with the case where an incident beam passes through the crystal scattering X-rays on the other side. Far more commonly we need to visualize what is referred to as reflection of X-rays.

The situation for a single plane of atoms (represented by a row in two dimensions) reflecting an X-ray beam incident at relatively low angles is portrayed in Fig. 3.7. Rays 1 and 2 are moving toward the row of atoms in phase.  $X-X'$  and  $Y-Y'$  are wavefronts. Atoms  $A$  and  $B$  are stimulated by the incident rays to scatter in all directions. The incident beam, the normal to the reflecting plane, and the diffracted beam are all in the same plane.

How do we determine in what direction or directions the scattered beam or beams will constructively interfere and form a diffracted beam? First, we must remember that for constructive interference, reflected rays 1' and 2' must be in phase. To be in phase, they must be at exactly the same place in their sinusoidal cycling, which is the same as differing by one or more whole wavelengths (see Fig. 3.3) because if one gets ahead or behind the other, there will be destructive interference. Notice that  $AC$  and  $BD$  are the same length if  $\theta = \theta'$ , and we have given that as a condition, or

$$AC - BD = AB \sin\theta - AB \sin\theta = 0$$

Both  $AC$  and  $BD$  are related to  $AB$  in the same way, all of which says there is zero wavelength difference between rays 1-1' and 2-2' so we can expect a diffracted beam. Each atom in row (plane)  $R$  could scatter rays, and the same condition would hold: They would constructively interfere only when  $\theta' = \theta$ ,

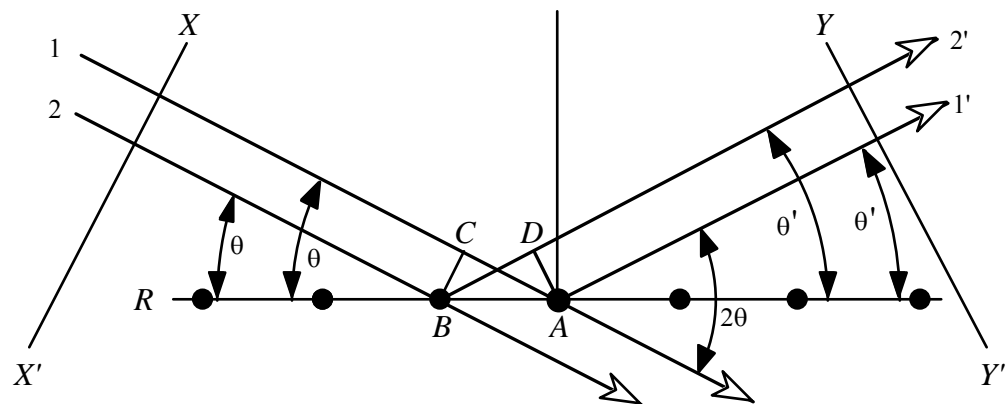


Fig. 3.7. Diffraction from a single row of atoms. 1 and 2 are incident rays; 1' and 2' are diffracted rays.

so there would be no phase difference. (This situation is very similar to that shown in Fig. 3.5; ray 2' is similar to line *de*, a line on a cone of diffracted rays, except in Fig. 3.7 the rays are shown originating at the atom instead of between pairs. This is a convenience for the graphics. The diffracted beams shown in Figs. 3.4 and 3.5 would have significantly less intensity than the diffracted beam of Fig. 3.6C.) For a single row, diffraction can take place at any angle with the condition that  $\theta' = \theta$ . This is the way visible light is reflected from a mirror. However, no crystals are this thin, so we must consider additional planes of atoms.

Figure 3.8 adds planes (again, represented in two dimensions by rows) of atoms *S* and *T* to the plane *R* shown in Fig. 3.7. Again, in order to have a diffracted beam, the rays at the wavefront *Y-Y'* must all be exactly in phase. From Fig. 3.8 it is obvious that some rays have traveled farther than others to reach *Y-Y'*. If rays 1', 2', 3', and 4' are to arrive at *Y-Y'* in phase with one another, rays 3', and 4', must have path lengths exactly one, two, or three (or some whole integer) wavelengths longer than rays 1', and 2'. If the rays satisfy this condition, they will be in phase with one another. You won't be too surprised that there is a way to express this geometrically. You can see that ray 3-3' has traveled farther than ray 1-1'. Do you see that the additional distance is *EG + GF*? This distance must equal some whole number of wavelengths. Now notice that the two triangles *EGA* and *FGA* have a common side *AG* that is also the spacing *d* between rows of atoms. Also notice that the angle *EAG* equals  $\theta$ . (Briefly, the proof is that *EA*, one side of angle *EAG*, is perpendicular to ray 1; the other side of the angle, *AG*, is perpendicular to row *R*. Then, because row *R* and ray 1 make the angle  $\theta$ , and because *EAG* represents a  $90^\circ$  rotation of this angle, the two angles are equal.)

To arrive at a simple equation that will relate angle of incidence, spacing between rows, and wavelength difference in terms of the wavelength of the incident X-rays, we need to express *AG* in terms of  $\sin\theta$ , and *EG* and *GF* in terms of an integral number of wavelengths. Therefore, see that  $\sin\theta = EG/AG$  (because *AG* is the hypotenuse of the triangle and *EG* is the side opposite the angle  $\theta$ ) and  $\sin\theta' = GF/AG$ , so  $AG\sin\theta = EG$  and  $AG\sin\theta' = GF$ . Then,

### Box 3.1. Diffraction and Reflection

Though the X-ray beam is really *diffracted*, the term *reflected* is in such common use that we will continue to use it here with the understanding that it is not reflection in the sense of visible light reflected by a mirror. The angle of incidence equals the angle of reflection, or diffraction, for X-rays and visible light. Reflection of X-rays differs from reflection of visible light in that visible light is reflected at all angles, whereas X-rays are reflected at only a very few angles rationally related to one another. And one more point: In general optics the angles of incidence and reflection are measured from the normal, whereas in X-ray diffraction the angles of incidence and reflection, or diffraction, are measured from the reflecting or diffracting plane.

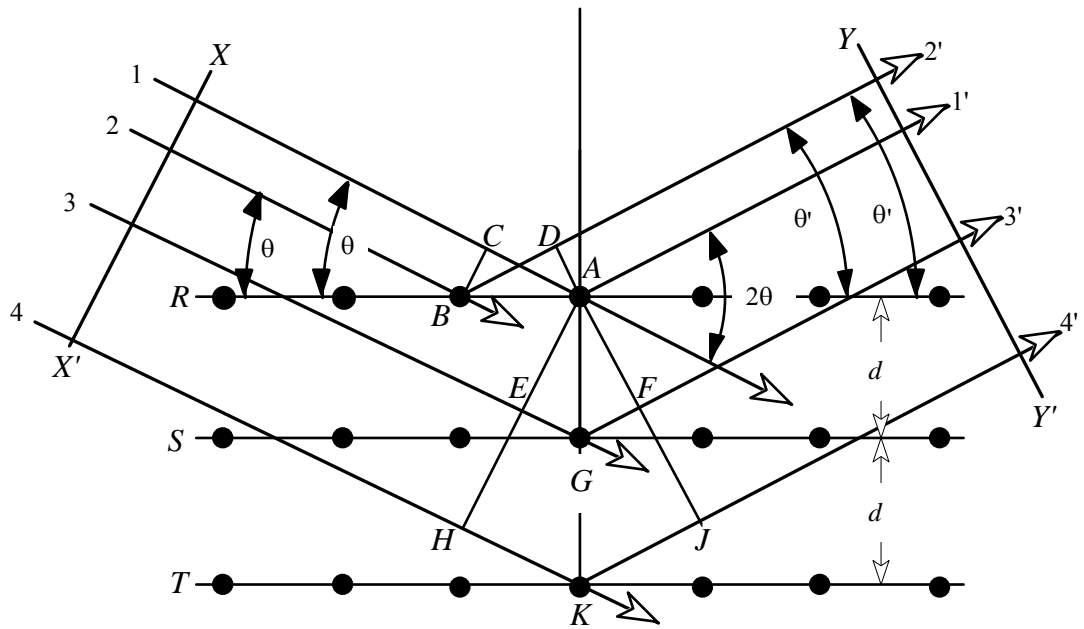


Fig. 3.8. Diffraction from more than one row of atoms illustrating Bragg's law. 1 is one ray of the incident beam; 1' is one ray of the diffracted beam;  $KGA$  is the normal to the planes causing diffraction; and the axis of the diffractometer is perpendicular to the page at  $A$ . There are two unit "cells" in this sketch, each marked by separation of equivalent planes by  $d$ .

because  $\theta = \theta'$ , we can put  $2AG\sin\theta = EG + GF$ ; substituting  $d = AG$ , we have  $2d\sin\theta = EG + GF$ . Then the wavelength difference that must equal some integral number of wavelengths  $n\lambda$  is equal to  $EG + GF$ , so

$$2d\sin\theta = n\lambda \quad (3.1)$$

(What is the wavelength difference between ray 1-1' and ray 4-4'? Work it out assuming the difference of ray 1-1' and ray 3-3' is  $n = 1$ . You should be able to draw Fig. 3.8 and derive this relation without referring to the text. If you can do that, you understand it.)

This equation (3.1) is Bragg's law or the Bragg equation, first worked out by W. L. Bragg in 1912 (Bragg, 1913). You may safely infer from the detailed manner in which we've developed this equation that it is important. You will see it frequently, sometimes in different forms, and you will find it very useful. It is *the* most important relation for the use and understanding of X-ray diffraction. [In W.L. Bragg's original paper (1913), he used the relation

$$a\alpha = h_1\lambda, \quad a\beta = h_2\lambda, \quad a(1 - \gamma) = h_3\lambda$$

where  $a$  is the side of the cube (unit cell),  $\alpha$ ,  $\beta$ , and  $\gamma$  are the cosines of incident radiation, and  $h_1$ ,  $h_2$ , and  $h_3$  are integers. Are these direction cosines? Can you relate these equations to the development shown in Fig. 3.6?]

## THE ARITHMETIC OF SCATTERING

### *The Summation of Scattering Amplitudes*

Now we need to return to scattering and discuss scattering from a unit cell. To briefly review, we considered scattering by the electrons around an atom and concluded that we could assume that each atom was a point source sending out spherical wavefronts. Upon considering atoms in rows (two-dimensional array, Fig. 3.4), we find that there are only a few directions, not all possible directions, in which diffracted beams are formed by constructive interference of these spherical wavefronts. In three-dimensional arrays the diffracted beams represent much more constructive interference—more beams composed of more rays interacting, causing much more intensity (Fig. 3.6). You were asked to picture a family of diffracted beams emanating from each atom. In what follows we will get a bit closer to what really happens. For an incident beam at a Bragg angle, you will be asked to picture a single resultant diffracted beam emanating from each unit cell. Each of these beams will constructively interfere with its counterpart from every other unit cell. To describe the entire diffracted beam, we need to describe a beam from just one unit cell.

Just as the scattering efficiency  $f$  of an atom is somewhat less than the sum of the scattering from individual electrons because the beams from individual electrons are slightly out of phase with one another, so the scattering efficiency  $F$  of a unit cell is always less than the sum of the scattering of the individual atoms in the unit cell because the beams that the individual atoms scatter are usually at least partially out of phase with one another unless the diffraction angle is zero.  $F$ , then, is a measure of the intensity of the diffracted beam we observe. Because its value depends on the way atoms are arranged in the unit cell (the physical distance between them determining how much their scattered rays will be out of phase),  $F$  is called the *structure factor*. To find  $F$ , we need to sum the amplitude  $f$  of the beams scattered from each atom in the unit cell adjusted for the amount of interference caused by phase differences,  $\phi$ . (And phase differences will be directly related to how the atoms are placed in the unit cell. See Fig. 3.21 and Table 3.1 at the end of this chapter.) Phase differences are measured relative to one atom designated as the origin of the unit cell. In order to be compatible with our calculations, we need to express phase differences for interacting beams in terms of radians. We need to do all these things in order to select equations that experience has shown are useful. With the proper equations we can model the diffraction of X-rays; i.e., we can calculate X-ray diffraction tracings.

You may remember that when representing harmonic or wave motion, the wave or ray is represented by a sine wave, and a point on the wave can be described in terms of its *phase angle*,  $\emptyset$  (Fig. 3.9B or C). The phase angle can be expressed in terms of a fraction of a circle, which is  $360^\circ$ , or  $2\pi$  radians, as indicated by the sine wave in Fig. 3.9A. At point *a* in Fig. 3.9A the phase angle of the sine wave is said to be  $0^\circ$ ,  $60^\circ$  at *b*, and  $180^\circ$  at *c*. Using radians instead of degrees, point *a* would be at 0 rad, *b* at  $(60/360)(2\pi) = (0.167)(6.28) = 1.047$  rad, and *c* at 3.14 rad.

We also need to make use of vectors. Recall that vectors can be plotted on an *X-Y* coordinate system. The amplitude of a wave can be represented by the length of a vector, and the phase angle is represented by the angle between the *X* axis and the vector (see vectors  $\mathbf{A}_1$ ,  $\mathbf{A}_2$ , and  $\mathbf{A}_3$  and phase angles  $\emptyset_1$ ,  $\emptyset_2$ , and  $\emptyset_3$  in Fig. 3.9B). For two waves, the resultant vector  $\mathbf{A}_3$  representing the resultant amplitude and the resultant phase angle  $\emptyset_3$  can be found by simply adding the initial vectors  $\mathbf{A}_1$  and  $\mathbf{A}_2$  by the parallelogram law.

You may or may not recall that physicists and mathematicians find it convenient for problems of this sort to refer to the *X* axis as the axis of real numbers and the *Y* axis as the axis of imaginary numbers, and that any point in this *X-Y* space is called a complex number. The unit of measure along the axis of imaginary numbers is *i*, which is defined as the square root of negative one,  $i = \sqrt{-1}$ . (For further information see, e.g., Vance, 1963, pp. 417ff.) The reason for introducing complex numbers is that complex exponential functions may be used to describe both phase and amplitude in the same equation.

In the development that follows, the primary goal is to help you understand how the diffracted beam is a consequence of both the kinds of atoms present and their positions within the unit cell. To that end, there is an arithmetic problem at the end of this chapter that will allow you to see how to simulate, or model, an X-ray diffraction tracing. There are several equivalent

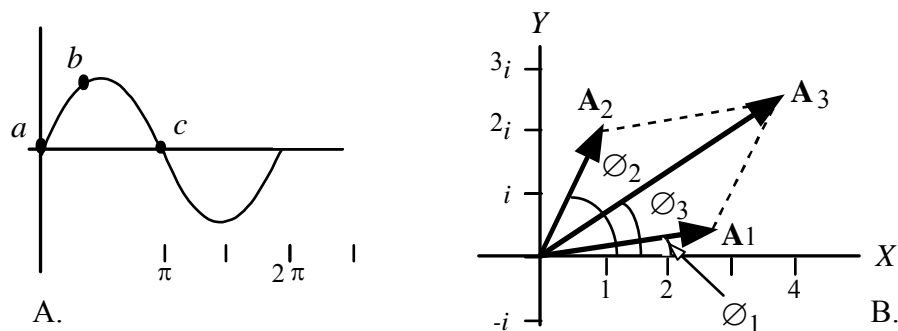


Fig. 3.9 A and B. Diagrams to aid in understanding the sine wave, radians, vectors, and complex numbers. See text for discussion.

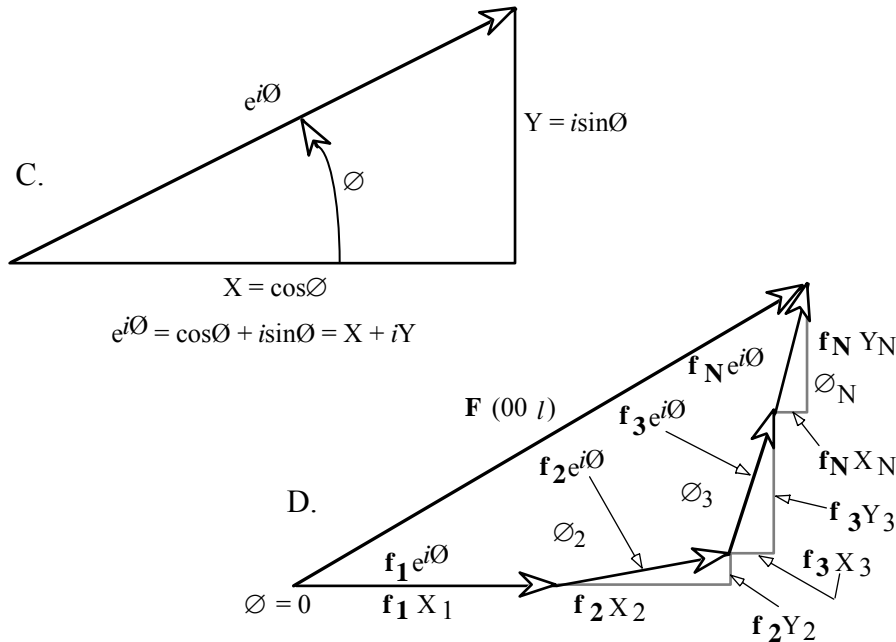


Fig. 3.9 C and D. Diagrams to aid in understanding the sine wave, radians, vectors, and complex numbers. See text for discussion.

mathematical paths to solving this problem. They all do the same thing—they add amplitudes in accordance with phases of the diffracted beams. A complex exponential function is presented in what follows, but most of the development is carried out using trigonometric relations. Our development is not comprehensive. There are several jumps in the logic, and some steps are taken by analogy rather than by rigorous mathematical reasoning. The goal is to offer you enough so you may gain insight into the process and a degree of faith in the development. See Chapter 2 in James (1965) or Klug and Alexander (pp. 152ff, 1974) for a more complete, rigorous development.

To begin our development, recall that there are very particular geometric constraints that must be satisfied before diffraction can take place. The incident and reflected beams must be in a plane perpendicular to the planes of atoms responsible for the scattering. In Fig. 3.10, the (00*l*) planes are perpendicular to the page and parallel to the lines of print. Now, assume that diffraction takes place from these (00*l*) planes, that *A*, *B*, and *C* are lattice positions occupied by atoms in a unit cell, and that for a beam incident at angle  $\theta$ , the Bragg law is satisfied. We know then that *DC* + *CE* must make the path of ray 2, which is scattered from the atom at position *C*, some whole number of wavelengths longer than the path of ray 1 scattered from the atom at position *A*. Another way to say this is, because the Bragg law is satisfied, *DC* + *CE* must be  $n\lambda$ , and we will assume  $n = 1$  for this argument. Then, from Bragg's law, the wavelength difference between rays 1' and 2',  $\Delta_{1'2'}$  is

$$\Delta_{1'2'} = DC + CE = \lambda = 2d(001)\sin\theta$$

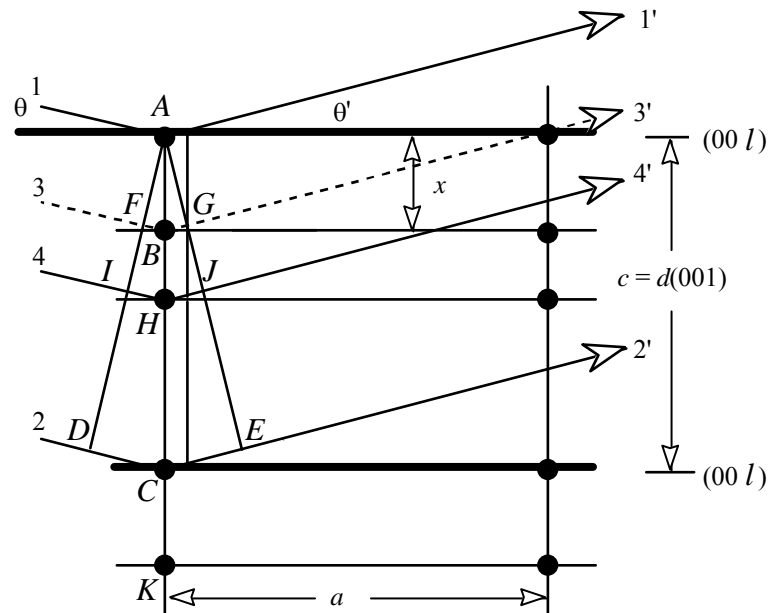


Fig. 3.10. Diffraction from a two-dimensional unit cell, assuming an orthogonal cell.

Now we ask how scattering from the atom at position B will affect scattering from atoms A and C. Certainly  $FB + BG$  must be less than  $1\lambda$ , if  $n = 1$ , and therefore the ray scattered from atom B will be out of phase with rays from atoms A and C. (Because A and C are equivalent positions in this unit cell, they must be occupied by the same kind of atom, and likewise, atoms B and K must be the same but not necessarily the same as A and C. The distinction between positions and the atom at that position will now be dropped with the understanding that this distinction is valid but inconvenient.) How much out of phase? Do you see that because the rays scattered by atoms A and C are exactly one wavelength apart and therefore in between rays 1' and 3',  $\Delta_{1'3'}$  is

$$\Delta_{1'3'} = (AB/AC)\lambda = (FB + BG)/(DC + CE)\lambda$$

In anticipation of where we are going with this development, we substitute  $x$  for  $AB$  and, from the definition for Miller indices,  $AC = c/l$  (see Fig. 3.10). Then

$$\Delta_{1'3'} = [x/(c/l)]\lambda$$

Now we need to express this phase difference in terms of angular measure or radians by multiplying the phase difference by  $2\pi/\lambda$  (there are  $2\pi$  radians per wavelength or per complete cycle on a sine wave, as in Fig. 3.9A). Now we don't need to know the wavelength to express phase difference (see below that  $\lambda$  cancels out).

$$\emptyset = (\Delta_{1'3'})2\pi/\lambda$$

Do you see that if  $\Delta$ , the difference in distance the two waves travel, is equal to  $\lambda$ , then  $\emptyset$  equals  $2\pi$ , which equals  $360^\circ$ , and the waves would be perfectly in phase? From above

$$\emptyset = (\Delta_{1'3'})2\pi/\lambda = [x/(c/l)\lambda](2\pi)(1/\lambda) = 2\pi l(x/c)$$

Recall that fractional coordinates in a unit cell are expressed as  $(uvw)$ . Then because  $x/c$  is a fractional coordinate,  $x/c = w$ , and

$$\emptyset = 2\pi lw \quad (3.2)$$

If we consider this relation for three dimensions  $(hkl)$  instead of the one dimension, we have

$$\emptyset = 2\pi(hu + kv + lw)$$

This general relation is applicable to a unit cell of any shape. But because we often work with clay minerals oriented so that diffraction will take place only from the  $00l$  spacings (at least that's what we try to do), the development is easier to follow, and the following development will be made in terms of the  $00l$  diffraction series.

The development above is OK for orthogonal cells, but, as you're aware, there always are complications. For monoclinic or triclinic cells,  $c$  is still the unit cell dimension along the monoclinic axis, but is no longer perpendicular to  $d(001)$ , but is now equal to  $c\sin\beta$ , or, if you'll look ahead to the section on reciprocal lattice,  $c^*$  is the reciprocal unit cell dimension along  $Z^*$ . Invariably, in the figures and in our thinking, we visualize the atom positions in the cell as arrayed along the normal to  $d(001)$  as in Fig. 3.20, and this dimension is  $Z^*$  or  $c\sin\beta$ .

### ***The Structure Factor F***

We have now developed an expression to describe phase differences for the beams scattered by atoms  $A$  and  $B$  in Fig. 3.10 [Eq. (3.2) and its general form]. This equation is applicable to atoms in all planes causing diffraction, but there are also differences in the amplitude  $A$  of each beam. We need to return to the atomic scattering factor  $f$  (p. 72), which is a ratio of the amplitude from an atom to that from an electron

$$f = \frac{\text{Amplitude of a wave scattered by the atom in question}}{\text{Amplitude of a wave scattered by an electron}}$$

We need an expression that will give us the phase and amplitude of the single diffracted beam that results from combining the phases and amplitudes from the waves scattered by each of the atoms making up a unit cell. One way to see this is from Fig. 3.10, from which we can imagine summing the atomic scattering factors  $f$  and the phase angles  $\emptyset$  for each of the atoms of the unit cell,  $f_a, f_b, \dots, f_n$  and  $\emptyset_a, \emptyset_b, \dots, \emptyset_n$

$$F(00l) = \Re \sum_n (f_n, \emptyset_n) \quad (3.3)$$

$F$  is the structure factor defined on p. 72.

Equation (3.3) is too general to be of much use. Therefore, we need to develop it into some form that will allow us to calculate the intensity of a diffracted beam. Referring again to Fig. 3.9B, note that the length of the resultant vector and its angle with the  $X$  axis can be described in trigonometric terms but, because the  $Y$  axis is imaginary, the imaginary number  $i$  is introduced. The equation  $e^{i\emptyset} = \cos\emptyset + i\sin\emptyset = X + Yi$  (Fig. 3.9C) is the well-known Euler identity. Figure 3.9D is called an Argand diagram and is directly applicable to our problem. It is a more involved form of Fig. 3.9C.  $F(00l)$  is a vector representing the phase and magnitude of the amplitude of a resultant wave. It is formed from the summing of a set of vectors representing the contributing waves, each with its scattering factor  $f_n$  and its phase angle  $\emptyset_n$ . The same operation can take the form of an exponential sum

$$\begin{aligned} F(00l) &= f_1 e^{i\emptyset^1} + f_2 e^{i\emptyset^2} + f_3 e^{i\emptyset^3} + \dots + f_n e^{i\emptyset^n} \text{ or} \\ &= \Re \sum_n f_n e^{i\emptyset^n} \end{aligned} \quad (3.4)$$

This equation (3.4) is more useful than Eq. (3.3) because it has established solutions. Then, using the identity given in Fig. 3.9C,  $e^{i\emptyset} = \cos\emptyset + i(\sin\emptyset)$ , we have

$$F(00l) = \Re \sum_n f_n \cos\emptyset_n + i \Re \sum_n f_n \sin\emptyset_n \quad (3.5)$$

When a center of symmetry is present in the unit cell and the origin for the calculation is set on that center, the sine series equals zero and the sine function is eliminated along with the imaginary number  $i$ . Because there is a center of symmetry on projection to  $Z$  for most clay minerals, the sine term drops out and we have the useful result (lucky us)

$$F(00l) = \Re \sum_n f_n \cos\emptyset_n = \Re \sum_n P_n f_n \cos(2\pi l z_n / c) \quad (3.6)$$

The second summation of Eq. (3.6) shows the expanded form of  $\emptyset$  [from  $\emptyset = 2\pi l (z/c)$ ].  $P_n$  is the number of atoms of type  $P$  per atomic layer,  $f_n$  is the scattering power of each of them,  $l$  is the order of the reflection,  $z_n$  is the displacement of the atomic layer, in Ångstroms, from the center of symmetry measured along a line normal to the  $(00l)$  plane, and  $c$  is the unit cell length. The intensity, which is what the detector measures, is (neglecting Lorentz-polarization effects) equal to  $|F(00l)|^2$ . Squaring  $F$  eliminates its sign; so we don't know whether  $F$  is positive or negative; we can only measure its magnitude.

Some structures have no center of symmetry on projection to  $Z$ . Then the intensity  $I$  is given by

$$I(00l) = |F(00l)|^2 = \left[ \sum_n \Re P_n f_n \cos(2\pi l z_n / c) \right]^2 + \left[ \sum_n \Re P_n f_n \sin(2\pi l z_n / c) \right]^2 \quad (3.7)$$

[This result is obtained by multiplying Eq. (3.5) by its complex conjugate,<sup>1</sup> thus eliminating  $i$ .] In this case, we can't talk about  $F$  as simply positive or negative, because it is a complex number. Now we turn to a consideration of the uses of the information gained from intensity.

### ***Information from Intensity***

Not all reflections are of the same intensity, not even those from the same set of diffracting planes, i.e., from the  $(00l) = (001), (002), (003), \dots, (00n)$ . In fact, there are some useful systematic absences (and variations) in the intensity from different members of a set of planes. These tell us something about the positions of atoms in the unit cell. We deal with essentially one dimension of the unit cell in the case of diffraction from clay minerals when we deliberately try to orient them on our sample mounts. If our orientation is perfect (and that never happens) only the  $(00l)$  spacings contribute to the diffraction pattern. By using the simplified situation in Fig. 3.10, you can see how the odd and even members of the  $(00l)$  series of spacing can account for the presence, absence, or variation of diffracted intensity. This same reasoning applies, of course, when interpreting X-ray tracings from random powder mounts.

Return to Fig. 3.10 with its five rows with atoms, A, B, C, H, and K. First, picture the diagram without the row of atoms H so that  $d$  is from the plane of atoms A to that of atom C. Next, imagine that ray 2-2' is exactly in phase with ray 1-1' because  $DC + CE = 1\lambda$  so that there will be diffracted intensity. This is the first case. Now, if we place the row with atoms H exactly halfway between rows with atoms A and C (i.e.,  $d$  is still the same), do you see that  $IH + HJ$  will equal  $l/2$ , and that, therefore, ray 4' will be perfectly out of phase

<sup>1</sup>The complex conjugate of, e.g.,  $A + iB$  is given by  $A - iB$ .

with rays 1' and 2'. If we imagine that atom H is exactly the same as atoms A and C there will be no diffracted intensity? (If the cell dimension  $c$  is really as shown in Fig. 3.10, why is it not possible for H to be the same as A and C?)

Remember that a spacing can cause diffraction at more than one angle. [When working with glycol-saturated Na-smectite, for example, its 17 Å (001) spacing will produce diffraction at 12 to 14 angles, i.e., give reflections for (00 $l$ ) spacings as high as (00,12) to (00,14). A few of the less intense (00 $l$ ) peaks are undetectable.] Again in reference to Fig. 3.10, the Bragg angle for rays 1 and 2 is about 30°. Leaving the row with atoms  $H$  in place, picture rays 1 and 2 incident at about 60° or high enough so that ray 2-2' would travel exactly  $2\lambda$  farther than ray 1-1'. Then ray 4-4' would travel  $1\lambda$  farther than ray 1-1' instead of  $\lambda/2$  as in the first case. (Try drawing this to see if it makes sense.) In this case, ray 4' would constructively interfere with rays 1' and 2', and diffraction would be observed, whereas when the diffracted ray 4' traveled only  $\lambda/2$ , it would destructively interfere with ray 1' and 2' and no diffraction would be recorded. In the first case, i.e., Bragg angle = 30°, we refer to the spacing from which there could be diffraction if row  $H$  were not present as (001), and in the case in which ray 4-4' traveled  $1\lambda$ , we call the spacing and the peak it forms on the diffraction tracing (002). From all this we generalize for the case with  $H$  present that we have no diffraction when  $l$  is an odd number, (00 $l$ ) = (001), and we do have diffraction when  $l$  is an even number, e.g., 002, 004.

In our example we assumed that atoms  $A$ ,  $C$ , and  $H$  were all the same. If, however, atom  $H$  is different, and had different scattering efficiencies  $f$  than atoms of  $A$  and  $C$ , then there could be observable peaks for the odd-ordered reflections and the intensity would be a function of how different the atoms were in atomic number and hence scattering factor. For example, if atoms  $A$  and  $C$  were Si and  $H$  were Al, there would be little difference in their scattering efficiencies because they have 14 and 13 electrons, respectively, or 10 and 10 as ions. There would still be no observable peaks for odd-numbered (00 $l$ )'s. If  $H$  were Fe, and  $A$  and  $C$  were Si, there would be a large difference in their scattering powers, and even after the amplitudes of the waves from the Si atoms were subtracted from those of the Fe, there would be sufficient intensity to show peaks for odd-ordered reflections. The situation in which this probably will be of most use to you is in distinguishing Mg and Al-rich chlorites from Fe-rich chlorites (see Chapter 7, pp. 233ff and Fig. 7.5). (Do you see that we could have used Fig. 3.8 as a basis for this discussion?)

The same reasoning applied to three-dimensional unit cells leads to similar generalizations that are helpful in determining lattice type in the study of crystal structures. For example, in the isometric system, structures with the simple Bravais lattice may have reflections from all possible sums of the ( $hkl$ ) values. Those with face-centered lattices may have reflections for  $h$  and  $k$  or for  $k$  and  $l$  that are both even or both odd, but reflections are not possible when  $h$ ,  $k$ , and  $l$  are mixed odd and even. For body-centered lattices,

reflections might be present when the indices add to an even number, but no reflections are possible when the indices add to an odd number. Cullity (1978, pp. 115-26) offers a detailed discussion of these relations. He also carries through, as a specific example, the calculation for the  $F$  of NaCl, a face-centered cubic structure. You might like to try following his exercise.

Deducing the kind of atoms and their positions from intensity data constitutes an analysis of structure. In classical X-ray crystallography such an analysis was all that was desired. For the clay minerals and some other substances, however, we need and can obtain other types of information on the size and perfection of the crystallites. In addition, for any X-ray diffraction study, there are certain instrumental and geometric factors that “get in the way,” so to speak, and we must take these into account. After discussing other factors that influence the amount of intensity we can observe, we will offer you some specific calculations to illustrate the effect of some of these factors.

### ***The Reciprocal Lattice***

We are sure that no one reading this has ever tried to impress anyone with their erudition by dropping words like post-modern deconstruction, Kierkegaard’s existentialism, . . . etc. Unfortunately, reciprocal lattice has joined this company of things we have designated as unapproachably abstract, something difficult to master, whereas it is actually relatively simple. It was invented in the summer of 1912 by Ewald (1921; 1962, p. 42) immediately after von Laue’s discovery, and helps us understand the distribution of diffracted intensity in space. Granted that it is an abstraction of an abstraction, it is quite simply derived from the lattices, the first ab-straction, that we use to describe the arrangement of atoms in the structures of crystals. We will present it in two steps. The first follows immediately, and the second will be in Chapter 10 in the discussion of diffracted intensity in three dimensions.

Not many mineralogists use film to record the diffracted beams of X-rays anymore, but you will see electron diffraction recorded this way. We’re sure you can picture a film with spots arranged in a symmetrical pattern. Each spot represents a beam of X-rays diffracted from a specific set of  $hkl$  planes in the crystal. Therefore, the spot also represents the geometrical position of a family of  $hkl$  planes in the crystal and the distance  $d$  between those planes, or an integer fraction of  $d$ . (And the density of the spot is a measure of the intensity.) That’s a lot of information in one spot.

To label and analyze all of the spots, there is need of an organizational framework. Start by picturing a simple unit cell, let’s say a monoclinic one. The cell is defined by edge lengths  $a$ ,  $b$ , and  $c$  along axes  $X$ ,  $Y$ , and  $Z$  (Fig. 3.11A). To define the coordinates of reciprocal space, image an axis  $X^*$  (we say  $X$  star) perpendicular to the (100) plane<sup>2</sup>, an axis  $Y^*$  perpendicular to the

<sup>2</sup>If you need to refresh yourself on crystallographic notation, see **Box 4.1 Nomenclature**, in

Chapter 4, p.133.

(010) plane, and an axis  $Z^*$  perpendicular to the (001) plane. These three axes form a reference framework that is the reciprocal of the one defined by  $X$ ,  $Y$ , and  $Z$ . The unit cell in reciprocal space is marked off by

$$a^* = 1/d(100), \quad b^* = 1/d(010), \quad \text{and} \quad c^* = 1/d(001), \quad (1/d) = d^*$$

where  $d$  is the same as in Bragg's law, the spacing between planes (Fig. 3.11B). Angles in real space are represented in reciprocal space by their supplements. Thus if the monoclinic angle  $\beta$  is  $100^\circ$ , then  $\beta^*$  (in reciprocal space) is  $180 - 100 = 80^\circ$ . The feature of clay minerals that we work with the most is, of course, their  $00l$  spacings. Let's use the  $10 \text{ \AA}$   $d(001)$  of illite as an illustration. If  $d(001) = 10 \text{ \AA}$ , then  $c^*$ <sup>3</sup> must equal  $1/10 \text{ \AA}$ . So, along the axis normal to the (001) of an illite crystallite, we mark off points at  $n1/d(001)$  along  $Z^*$  or  $1/10 \text{ \AA}$ ,  $1/5 \text{ \AA}$ ,  $1/3.33 \text{ \AA}$ , . . .  $n/10 \text{ \AA}$ . (Likewise, if we wished to work in the other two dimensions, units of  $a^*$  can be marked off along  $X^*$ , and units of  $b^*$  marked off along  $Y^*$ .) Crystallographers refer to these points as nodes. The scale of the reciprocal lattice is impossibly small for the first few values on  $n$ ; so we ignore scale and pretend it is just about the same as the scale we use to show the crystal structure. We can, of course, convert the other two principal directions in the crystal into their reciprocal equivalents.

Figure 3.11 is too busy, but should prove helpful in understanding some of this stuff. Let us take you through it step by step. Figure 3.11A is the two-dimensional part or  $XZ$  plane of the lattice for an ideal monoclinic crystal structure and shows two members of the 302 family of planes. Figure 3.11B shows the reciprocal lattice for the regular lattice shown in Fig. 3.11A. Now the 302 family of planes is represented by a spot and  $O^*P$ , a vector the length of which is  $1/d(302)$  or  $d^*(302)$ , is perpendicular to the (302) family of planes. In addition, it can be shown (but what we mean is, will you take this on faith from us?) that a line drawn from  $O^*$  (Fig. 3.11B and C) to any  $hkl$  node in the reciprocal lattice is perpendicular to the family of ( $hkl$ ) planes in the real crystal. Furthermore, the distance from  $O^*$  to the  $hkl$  node =  $d^* = 1/d$ . In other words, to relate this to something with which you are familiar, picture the illustrations used to explain the stereographic projections you learned to use in mineralogy. For these, you pictured a crystal at the center of a sphere with lines perpendicular to each crystal face extending to the surface of the sphere where the crystal face was represented by a point. The reciprocal lattice system is quite similar.

Because our application differs from former uses of the reciprocal lattice, we need to describe two ways in which it can be visualized. The conventional way to use this graph (Fig. 3.11C) is to ask you to imagine  $O^*$  as the origin of the lattice,  $C$  as the point at which diffraction occurs in the real crystal,  $CO^*$

<sup>3</sup>Note that  $c^*$  is a dimension along  $Z^*$  and not a direction. Therefore we shouldn't use the  $c^*$  when we mean a direction perpendicular to  $d(001)$ , and  $Z^*$  is perpendicular to  $d(001)$  by

definition.

parallel to, and as an extension of, the incident beam, and the direction of the diffracted beam represented by  $CP$ . If we have a randomly oriented powder sample, there should be at least one crystal oriented so that its reciprocal lattice is in the position shown in Fig. 3.11C. Then, any time a crystallite is in an orientation that puts a node of its reciprocal lattice on the circle (or sphere in three dimensions, this is called the Ewald sphere of reflection) that has a radius of the reciprocal of the wavelength of the incident ray  $1/\lambda$ , Bragg's law is satisfied and diffracted intensity will be obtained. Ewald's method of finding diffraction intensity was to rotate the reciprocal lattice to see which nodes intersected the surface of the sphere for each increment of  $\theta$ . [Later in this chapter we will point out that to get the right amount of intensity at a node, the intensity intercepted will have to be multiplied by the structure factor for this node, i.e.,  $F(hkl)^2$ .]

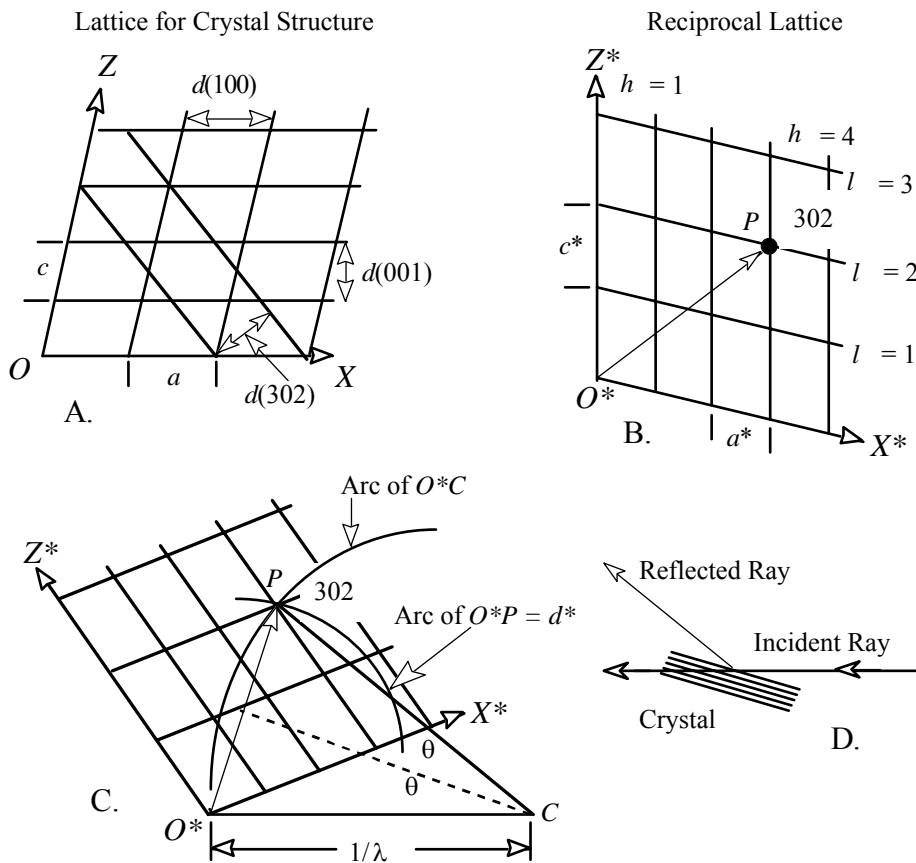


Fig. 3.11. Diagrams to help understand the reciprocal lattice. A. Two-dimensional view of a monoclinic lattice. B. The reciprocal lattice derived from A showing the node for 302. The line  $O^*P$  equals  $1/d(302)$ , and is perpendicular to the 302 planes of A. Notice that the  $h$  and  $l$  values are marked on B. Do they read correctly for the 302 node? C. The geometric condition for satisfying Bragg's law for  $d(302)$  and to show the arcs made by the two radii,  $O^*C$  and  $O^*P$ . Bragg's law is developed below. D.

Sketch of the crystal responsible for the reflected ray  $CP$  in C.

A method suggested by Brindley and Méring (1951) for identifying the distribution of diffracted energy uses this same construction (Fig. 3.11C) but sweeps through a sphere of radius  $d^*$  originating at  $O^*$ . In this variation, the reciprocal lattice does not move and diffracted intensity is sought with the sweep of the  $d^*$  radius for each increment of  $\theta$ . Arcs of both spheres are shown in Fig. 3.11C. To calculate all the diffraction intensity that could occur within a diffraction scan, the integrated intensity within each increment of  $2\theta$  is plotted against  $2\theta$  (see Chapter 10). Figure 3.11D shows you the parallel relation of the incident ray to  $CO^*$  and the reflected ray to  $CP$  in Fig. 3.11C.

To derive Bragg's Law (Eq. 3.1) from Fig. 3.11C, note that

$$O^*P = (2) (O^*C)(\sin\theta)$$

and because

$$O^*P = d^*, \quad d^* = (2) (1/\lambda) (\sin\theta)$$

$$\text{then } 1/d = (2) (1/\lambda) (\sin\theta)$$

and that is the same as

$$\lambda = 2d\sin\theta$$

which is, of course, Bragg's law (Eq. 3.1).

So, any time a crystallite is in an orientation that puts a node of its reciprocal lattice on the circle that has a radius of  $1/\lambda$  or  $1/d$ , Bragg's law is satisfied and diffracted intensity will be recorded. This approach is necessary to visualize diffraction from a randomly oriented powder instead of diffraction from a single crystal.

Now, although these arguments may not seem fully intuitive, and you may not yet be fully comfortable with them, we need to move on. We can use your understanding of the machinations related to Fig. 3.11C to deal with the peak shapes, missing or weak peaks of semidisordered clay minerals, the band shapes of the turbostratic and close to turbostratic clay minerals, and with the diffraction patterns produced by polytypes, all of which we will discuss in subsequent chapters. We will see this topic again in Chapter 10.

### REAL VERSUS IDEALIZED PEAKS ON XRD TRACINGS

We made simplifying assumptions to derive the Bragg equation (Eq. [3.1] and Fig. 3.8), as is always the case when we begin to model nature: (1) that the incident beam is perfectly monochromatic; (2) that the rays are perfectly parallel; (3) that we have only three rows of atoms and they are a perfectly ordered part of a perfect and infinite crystal; and (4) that the crystal is perfectly oriented for diffraction to occur. As we apply the Bragg equation to

diffraction tracings, we need to consider how real circumstances differ from the idealized ones. Figure 3.12 shows a real diffraction tracing, and Fig. 3.13 will help us understand some of the characteristics of the peaks shown on this tracing.

The first thing we consider is why diffraction peaks are so narrow or, said in another way, how destructive interference is produced in all directions except those of the diffracted beam. Recall that the condition for constructive or reinforcing interference is that the rays must be in phase and differ by some whole number of wavelengths (includes 0). In Fig. 3.3C, the two waves *R* and *S* interfere destructively; they are out of phase but do not completely destroy one another. Their amplitudes simply add to form a beam of smaller amplitude compared to those of Fig. 3.3B, which are in phase. If another wave, out of phase with *R* as much as *S* is out of phase, interacts with the combined amplitude of *R* and *S*, the amplitude is reduced more, and so on until there is no amplitude at all.

To understand the effect of destructive interference on the peak shapes we see in Fig. 3.12, we need to consider the contributions from planes deeper into the crystal. Let us refer to Fig. 3.13. The ray 1-1' scattered by the first plane

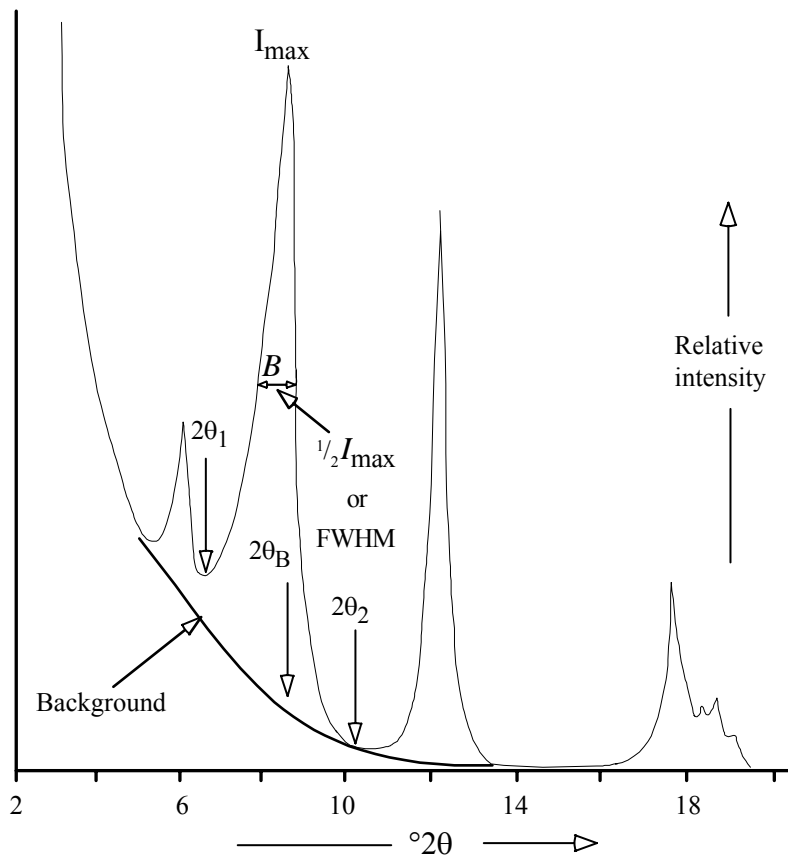


Fig. 3.12. X-ray diffraction tracing of the  $< 2 \mu\text{m}$  fraction of the Purington Shale from an oriented aggregate mounted on a glass slide, Cu radiation.  $2\theta_B$  is the Bragg angle

for the most intense peak,  $2\theta_1$  and  $2\theta_2$  are limiting angles as in Fig. 3.13, and FWHM = full width at half-maximum peak height above background.

below the surface has a path exactly one wavelength longer than ray 0-0'. Therefore, all rays reflected from planes in the crystal at an angle so that this condition is met unite to form a diffracted beam. This angle is known as a Bragg angle  $\theta_B$ . As the angular relation between the incident beam and the planes of the crystal shift to either slightly greater or lesser angles, angles that are close but not quite Bragg angles, rays reflected from all planes 0 to  $N$  will destructively interfere.

Consider rays  $A-A'$  and  $C-C'$ . Let's say ray  $C-C'$  is one and one-tenth wavelengths longer than  $A-A'$ . The amplitudes of  $A-A'$  and  $C-C'$  will add, but because they are out of phase by one-tenth of a wavelength, the resultant amplitude will be less than double the amplitude. The ray reflected from row 2 will be two-tenths of a wavelength out of phase with ray  $A-A'$ , and so on, until we reach row 5. The ray reflected here will be five-tenths, or one-half wavelength out of phase. The sum of the amplitudes of rays from rows 0 and 5 will be exactly zero; from 1 and 6, exactly zero; from 2 and 7, exactly zero; etc. If  $A-A'$  and  $C-C'$  were one-one hundredth out of phase, do you see that the sum of amplitudes from rows 0 and 50 would be exactly zero?

To generalize from this specific example, once there is the slightest deviation from the Bragg angle  $\theta_B$  then at some depth in the crystal, there will be a row  $N$  that reflects a ray that is exactly one-half wavelength out of phase

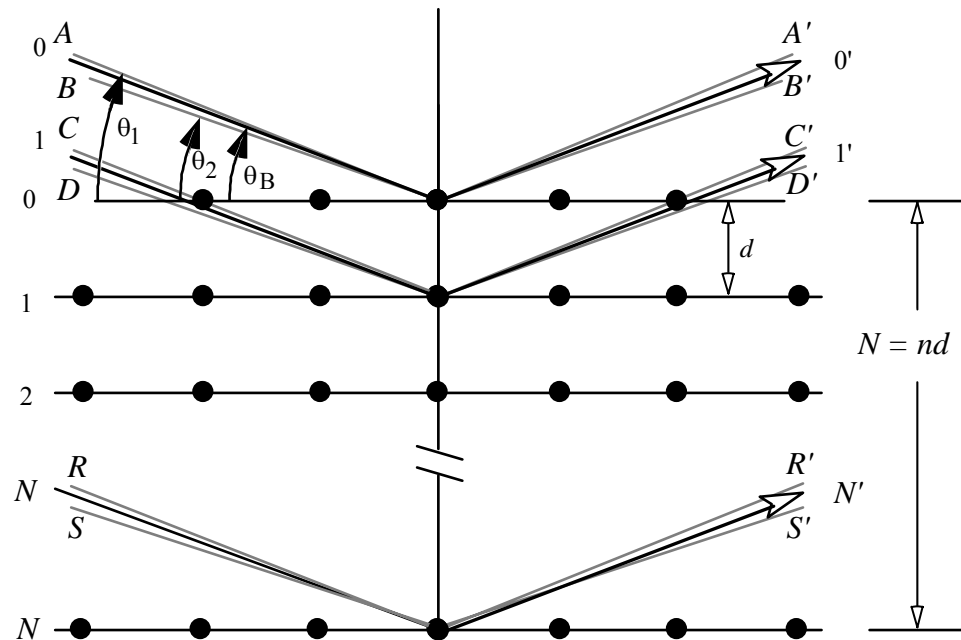


Fig. 3.13. Diffraction at a Bragg angle with two limiting angles at which there is destructive interference. The figure shows beams 0, 1, and  $N$ , and planes of atoms 0, 1, 2, etc., and  $N$ .

with the ray reflected from the top row 0. Further, row  $N + 1$  will be exactly one-half wavelength out of phase with row 1, and so on. You can see that the same argument applies to ray  $B-B'$  at an angle  $\theta_1$ , just less than  $\theta_B$ , so we have two limiting angles on either side of  $\theta_B$ ,  $\theta_1$  and  $\theta_2$ , when ideally the intensity should drop to zero. We can now see that peaks on diffraction tracings tend to be so narrow and sharp because *destructive interference is just as much a consequence of diffraction from a periodically repeating array of atoms as is constructive interference.*

Suppose now that the crystal represented in Fig. 3.13 contained only rows 1, 2, and 3. Then slight departures from  $\theta_B$  would not result in complete cancellation. There would be measurable intensity at these angles. In other words the peak would be broadened to include the beams at angles  $\theta_1$  and  $\theta_2$ , although they would have less intensity than that part of the beam at  $\theta_B$ . From this example you can see the reason that peaks get sharper as crystals get thicker, or contain more rows like  $N$ .

Based on this discussion, the question should arise, "Why is there any finite width to the diffraction peak at all if it is produced by a thick crystal?" There are several reasons, some of which will help you understand the real, as opposed to the ideal, nature of analytical procedures and minerals. First, although we assumed perfectly parallel incident rays and perfectly monochromatic radiation, neither is technically possible and both of these deviations from ideal add something to peak width. For Cu radiation, the  $K\alpha$  peak has a finite range of wavelength values of about 0.001 Å. For the peak at  $8.85^\circ 2\theta$  (representing a spacing of about 10 Å (does that work out right with the Bragg equation, p. 71?), the finite width of  $CuK\alpha$  radiation adds about  $0.002^\circ 2\theta$  to the peak width. Other instrumental factors are more weighty and guarantee that finite peak breadth will be observed for diffraction from any crystal studied by powder diffractometry. The diffractometer is an optical device, and, like all optical devices, it necessarily introduces distortion and defocusing into any image that it records. The effects can be minimized by careful alignment, proper slit selection, and perfectly flat samples that are perfectly aligned. The best compromise between resolution and intensity that you can achieve with modern diffractometers is a peak breadth at half height of about  $0.08^\circ 2\theta$ , and even that shows additional broadening at high values of  $2\theta$  due to separation of the  $CuK\alpha_1$ - $K\alpha_2$  components of the incident radiation. The latter can be eliminated by the use of certain monochromators which are rarely used in mineral analysis because they cause prohibitive intensity losses. Graphite monochromators are another matter, and these are almost standard today, but their resolution is insufficient to eliminate  $CuK\alpha_2$  radiation. For most clay mineral studies, you don't need this kind of resolution anyway because the minerals themselves produce broad peaks whose sharpness cannot be improved by any optical refinement.

A characteristic of all minerals is imperfection in crystal order, especially for clay minerals, because of their small crystal size. Almost all real crystals

have an imperfection known as mosaic structure (diamond and calcite can be exceptions). In real crystals, a row of atoms does not extend unbroken across the whole width of the crystal; only within small volumes is there perfect order. These small volumes join other small volumes close to, but not quite in, perfect alignment. The size of these mosaic pieces or subgrains is about 1000 Å or less, and the disorientation between adjacent subgrains is a matter of seconds to minutes of arc, seldom as much as 1°. Many clay minerals are often 1000 Å in the largest dimension and may have subunits within that distance. These small crystals, or crystallites for very small crystals, cause noticeable line broadening.

Particle-size broadening or, in our case, thickness of crystal, is conveniently inferred from the width of the peak at peak half-height (see Fig. 3.12) for the reasons discussed related to Fig. 3.13. It is used to estimate particle size and, under ideal conditions, the distribution of particle sizes. As we have seen, the width of the peak becomes broader for smaller particles. This is expressed quantitatively by the Scherrer equation

$$L = \frac{\lambda K}{\beta \cos \theta} \quad (3.8)$$

where  $L$  is the mean crystallite dimension in Ångstroms along a line normal to the reflecting plane,  $K$  is a constant near unity, and  $\beta$  is the width of a peak at half-height expressed in radians of  $2\theta$  (i.e., measure  $2\theta$  in degrees and then multiply by  $\pi/180$ ).

Another source of line broadening on which we merely comment is called *strain broadening*. This results from random displacements of unit cells or groups of unit cells from their ideal positions of perfect registry. It can be mathematically separated from the effects of particle-size broadening. The treatment is too complicated for the scope of this book, especially since it has yet to be demonstrated for clay minerals. Line broadening is treated briefly by Cullity (1978, pp.101-02) and in more detail in Klug and Alexander (1974, pp. 299-306 and Chapter 9).

The effect of “particle” size on the peak width for clay minerals has been called into question by work published by Nadeau et al. (1984), in which they show high-resolution transmission electron microscope (HRTEM) photographs of individual particles of smectite that are as small as 10 Å thick. The same smectite sample when deposited as an oriented aggregate gives diffraction peaks whose broadness indicates that there are on the average nine layers per scattering domain, or 90 Å. To resolve the discrepancy between the XRD and the HRTEM data, Nadeau et al. proposed that in preparing samples for X-ray diffraction, the 10 Å-thick particles stack together to make an array from which coherent scattering can be obtained. They call this effect *interparticle diffraction*.

A final cause of broad peaks is mixed layering, or interstratification, of different kinds of clay minerals. Several clay minerals, usually with different  $c$  dimensions, are frequently intergrown, and a resulting diffraction peak represents an averaging of the two spacings. We will look at this in more detail in the sections on characteristics of clay minerals (Chapter 5) and identification of mixed-layered clay minerals (Chapter 7).

***The Interference Function  $\Phi$ : Diffraction from a Crystal Whose Unit Cell Has a Unitary Scattering Factor***

For those working with large crystals, essentially infinite in thickness and more ordered than those of the clay minerals, the shape of the diffraction peaks carries little information. For larger crystals, only  $F$  is needed because almost all the scattering is concentrated at the Bragg angles of diffraction. However, for small, thin crystals such as those of the clay minerals, there is additional scattering adjacent to the  $hkl$  diffraction peak positions, as shown in the discussion of Fig. 3.13, and even in small amounts between these positions. (To date, most analyses of clay minerals have been based on peak position and intensity. Peak shape and breadth may become as important as peak position in the future.) Characteristics of diffraction peak shapes that result from this extra scattering, and their correlation with the nature of the crystalline aggregates of unit cells, can be separated from the structure of the unit cell itself, which is described by  $F$ . We simply set the amplitude of scattering ( $F$ ) from each unit cell equal to unity. Calculation of the diffraction pattern from any assemblage of such cells, using this additional scattering, is called the *interference function*, and it is given the label  $\Phi$ . Don't worry, though. When we want to return to the real world, we simply multiply the interference function by the appropriate value of  $F^2$  for each point on the  $2\theta$ -continuous profile of  $\Phi$ . But there is a problem here:  $F$  is defined by  $hkl$ . We need a formulation for  $F$  that yields the amplitude of scattering as a *continuous* function of  $\theta$ , not simply a value of  $F$  at a single  $2\theta$  value. The necessary alteration of  $F$  is greatly simplified by the one-dimensional case. The alteration we will use is essentially the same as  $F$  except that it is continuous with respect to  $\theta$ . It is the layer structure factor, or layer scattering factor  $G$ .

In addition, Eq. (3.6) must be converted to the units of  $\theta$ . To accomplish this, we make use of the Bragg relation  $n\lambda = 2d\sin\theta$  where  $d = d(001)$ . The analysis here is one-dimensional, so we can replace the order  $n$  in the Bragg law, with the index  $l$ . Rearranging gives  $l = 2d\sin\theta/\lambda$ . The  $d$  in this equation is equal to  $d(001)$  (which is different than the unit cell dimension  $c$ , if the symmetry is monoclinic or triclinic) and substituting  $2d\sin\theta/\lambda$  for  $l$  in Eq. (3.6) leads to [symbols as in Eq. (3.6)]

$$G(\theta) = \sum_n P_n f_n \cos(4\pi z_n \sin\theta / \lambda) \quad (3.9)$$

where  $z_n$  is the atomic coordinate times  $\sin\beta$ . Now we have an equation in terms of  $\theta$  instead of the index  $l$  and a scattering factor that is continuous ( $G$ ) instead of discontinuous ( $F$ ).  $F$  is reserved for the structure factor defined only at  $hkl$ . Crystallographers are tidy people who don't like ambiguities.

The interference function  $\Phi$  is also a continuous function and is given by

$$\Phi(\theta) = \frac{\sin^2(2\pi ND\sin\theta / \lambda)}{\sin^2(2\pi D\sin\theta / \lambda)} \quad (3.10)$$

where  $N$  is the number of unit cells stacked in coherent scattering array along the  $Z$  axis and  $D = d(001)$ . You can compute and plot diffraction profiles from this equation and verify that the breadths of the peaks at half-height do indeed square with the predictions of the Scherrer equation (3.8). The value of  $L$  in the Scherrer equation is equivalent to  $N$  times  $D$  in Eq. (3.10).

If we multiply  $G$  by  $\Phi$  for each increment of  $2\theta$ , we are pretty close to a final calculation of a complete one-dimensional X-ray diffraction pattern. However, two additional factors must be considered. Both factors vary with  $\theta$ . One is called the *polarization factor*, the other the *Lorentz factor*. Their combined effect is seen in Fig. 3.12, where the background and peak intensities at angles less than  $12^\circ 2\theta$  increase rapidly. A brief qualitative statement about both is given here. Detailed explanations for both factors can be found in Cullity (1978, pp.107-39) and Klug and Alexander (1974, pp.142-44).

### ***The Lorentz-Polarization Factors***

The polarization factor accounts for increases in peak and background scattering from a maximum at  $0^\circ 2\theta$  to a minimum at  $90^\circ 2\theta$ . The maximum effect on intensity is a factor of two. The basis for this change is that as radiation comes from the tube it is unpolarized, but the process of scattering causes a degree of polarization related to the angle of the incident and diffracted beams. The X-rays are polarized as they are diffracted from a plane of atoms for the same reason a beam of light is polarized by reflecting off the hood of a car, and polarized in the same way; i.e., the vibrations surviving the reflection are those parallel to the hood of the car or the plane of the atoms. As amplitude in directions other than that of the plane of polarization is lost, the intensity decreases. The total energy of the scattered beam is proportional to the polarization factor  $(1 + \cos^2 2\theta)/2$ , where  $\theta$  is the angle between the incident beam and the reflecting plane.

The Lorentz factor is a combination of two geometrical factors that we will deal with trigonometrically. The first factor is a formulation for the volume of the crystal that is exposed to primary irradiation. The second one relates the number of crystals favorably oriented for diffraction at any Bragg angle  $\theta_B$ .

The Lorentz factor is different for random powders and single crystals.

Reynolds (1976) discussed application of the Lorentz factor for basal reflections from clay minerals in oriented aggregates. He concluded that there are two cases. In the first, for diffractometers that have two Soller slits, the smaller the slit openings, the closer the random powder Lorentz factor is approached. In the second case, the more nearly perfect the orientation of the clay minerals on their substrate, the closer the single crystal Lorentz factor is approached.

The two portions of the Lorentz factor are combined with the polarization factor  $(1 + \cos^2 2\theta)/2$  and given in the following forms (neglecting overall factors of 2):

The Lorentz-polarization ( $L_p$ ) factor for random powders (integrated intensity)<sup>4</sup>

$$L_p = (1 + \cos^2 2\theta) / (\sin \theta \sin 2\theta) \quad (3.11)$$

The Lorentz-polarization factor for single crystals

$$L_p = (1 + \cos^2 2\theta) / \sin 2\theta \quad (3.12)$$

If you plot these functions and examine them, you will see that they are very different at low values of  $2\theta$ , so the question arises: "What is the best form to apply to oriented aggregates of clay minerals?" There is no exact answer to this question because usually the preferred orientation is unknown, and the correct  $L_p$  equation is somewhere between the two unique cases as given. Experience with clay mineral samples prepared by either the glass slide or the Millipore<sup>®</sup> transfer process indicates that a realistic average degree of preferred orientation is  $\sigma^* = 12^\circ$ , where  $\sigma^*$  is approximately the rocking angle of the sample about the goniometer axis; i.e., all of the intensity of a given  $00l$  peak is collected through the  $12^\circ$  arc indicating that the diffracting crystals are perfectly oriented  $\pm 6^\circ$  (see Reynolds, 1986). The solution of the Lorentz factor, using this value,  $\sigma^* = 12^\circ$ , suggests that the random powder form is appropriate for results from diffractometers that use two Soller slits. For instruments with one Soller slit, Eq. (3.13) provides a rough approximation for integrated intensities.

$$L_p = (1 + \cos^2 2\theta) / (\sin 2\theta \sin^{0.8} \theta) \quad (3.13)$$

It is not very good ( $\pm 15\%$ ), but it is much better than using either the random powder or the single-crystal versions. Attempts to improve on this approach are unwarranted unless the preferred orientation ( $\sigma^*$ ) is measured and the correct Lorentz factor calculated using the equation given by Reynolds (1986).

<sup>4</sup>For point-by-point corrections on  $2\theta$  continuous diffraction profiles, the correct  $L_p$  powder factor is  $1/\sin^2 \theta$ .

You have probably been asking yourself, “Where is all of this leading?” The answer is that computer programs have become available (e.g., Reynolds and Hower, 1970; Reynolds, 1980; Reynolds, 1985; Reynolds, 1994; and see Chapter 10 and the Appendix) that allow the simulation, or modeling, of X-ray diffractometer tracings. NEWMOD<sup>©</sup>, for example, is a powerful, interactive program for deciphering real tracings, because to model a tracing you have to think about which atoms are in what positions in the unit cell under consideration. Modeling is particularly helpful in analyzing diffraction patterns from mixed-layered clay minerals [i.e., the stacking of two or more kinds of layers with the stacking direction along a line perpendicular to (001)]. The modeling done here [except for that for identifying polytypes, measuring the (060), and the treatment in Chapter 10] assumes that oriented aggregates are used so that all diffraction is due to the (00 $l$ ) spacings. Then the scattering is reduced to a one-dimensional problem, which greatly simplifies the arithmetic. You will see the application of this program, NEWMOD<sup>©</sup>, in Chapters 7, 8, and 9, and a description of how it was written in the Appendix. The exercise in the section following the next one will illustrate how calculations are made.

### ***Putting It All Together—Building an 00 $l$ Diffraction Pattern***

We have discussed the three essential ingredients for modeling a diffraction tracing, the Lorentz-polarization factor, the interference function, and the scattering amplitude of the unit cell. All three change with the diffraction angle  $\theta$ , and the final diffraction pattern is simply the product of these three quantities. Let’s now generate some  $2\theta$ -continuous, one-dimensional patterns for illite.

The intensity is calculated by taking the products of the interference function  $\Phi$ , the layer scattering intensity  $G^2$ , and the Lorentz-polarization factor  $L_p$ , at each increment of  $\theta$

$$I(\theta) = [G^2(\theta)][\Phi(\theta)][L_p(\theta)] \quad (3.14)$$

We start with an examination of  $\Phi$ . Figure 3.14 shows the calculated results for illite that consists of crystals that contain five unit cells each, or  $N = 5$ . Note the broad peaks that represent the 00 $l$  diffraction series. We expect such broad reflections because of the very small crystallite thickness assumed here. The peaks are sharpened a great deal by increasing the crystallite thickness to 15 unit cells (Fig. 3.15). The following observations are in order: (1) The interference function produces peaks with equal areas for all 00 $l$  diffraction positions (including the 000) and (2) The peak breadth is inversely related to  $N$ .

The background contains  $N - 2$  weak, evenly spaced ripples. They result from the unrealistic assumption that diffraction occurs only from crystals made up of exactly 5 (or 15) unit cells. We can do something about this and

obtain more realistic patterns. The values calculated for  $\Phi$  so far describe a single crystal that is  $N$  unit cells thick, but if we multiply Eq. (3.10), the equation for the interference function, by  $1/N$ , the result applies to an infinitely thick aggregate of such crystals.

We can eliminate or minimize the spurious ripples in the interference function if we assume the array causing diffraction is composed of a series of crystallites with different values of  $N$ —a much more physically realistic proposition. Each of these crystallites will produce ripples at different positions; so the sum will become a smooth background if we add a sufficient number of thicknesses. Let  $q(N)$  be the proportion of crystallites of thickness  $N$  normalized so that the sum of all values of  $q(N)$  is 1. Equation (3.15) shows the final result.

$$\Phi(\theta) = \sum_{N=n_1}^{N=n_2} q(N) \frac{\sin^2(2\pi ND\sin\theta/\lambda)}{N\sin^2(2\pi D\sin\theta/\lambda)} \quad (3.15)$$

Figure 3.16 shows the results from a sum of equal proportions of crystallites for which  $N$  varies from 2 to 15. The ripples have been almost eliminated, and the shapes of the peaks have changed. They now are more peaked; the tails are broader for a given width at half-height. Their shape illustrates the dependence of the shape of a diffraction line on the distribution pattern of crystallite sizes that make up the hypothetical crystallite aggregate.

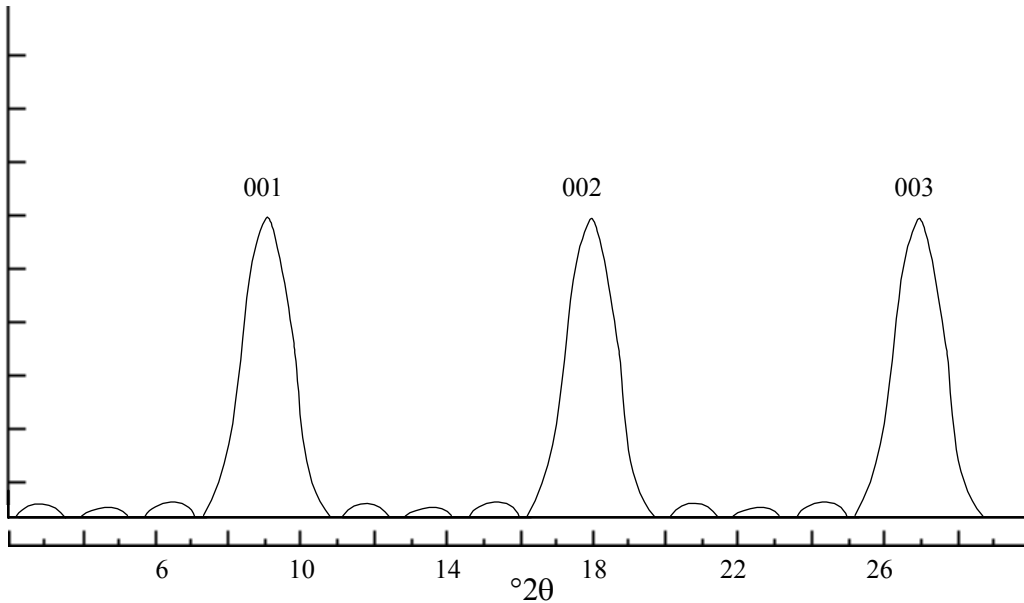


Fig. 3.14. Interference function ( $\Phi$ ) for  $N=5$ ,  $d(001) = 10 \text{ \AA}$ .

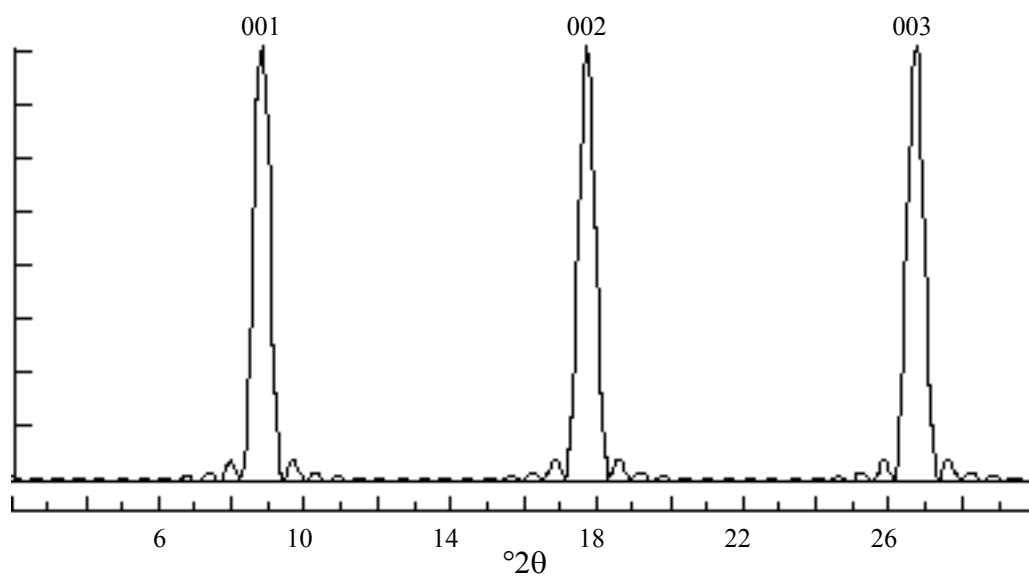


Fig. 3.15. Interference function ( $\Phi$ ) for  $N=15$ ,  $d(001) = 10 \text{ \AA}$ .

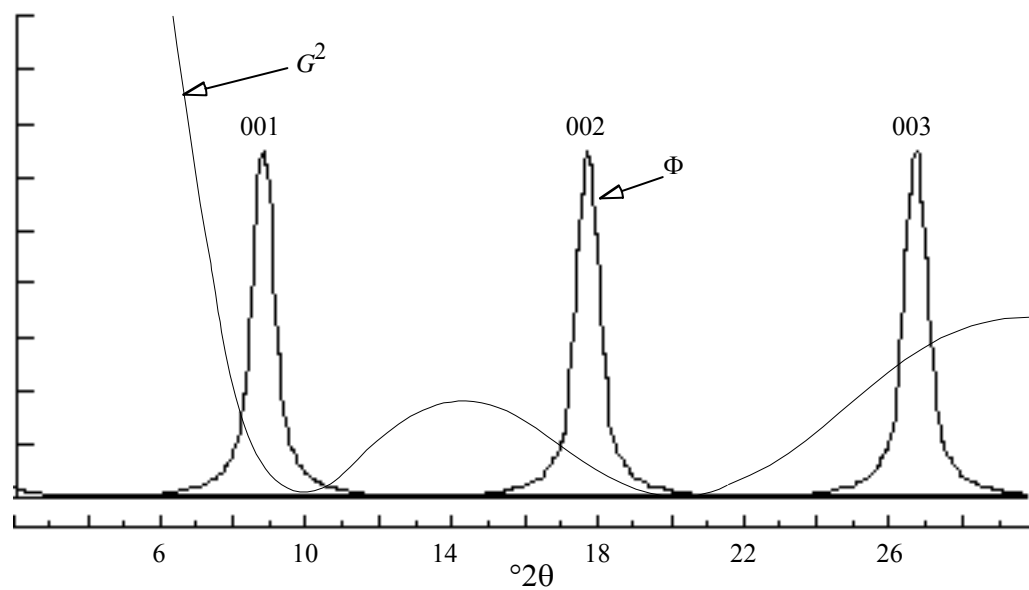


Fig. 3.16. Interference function ( $\Phi$ ) for  $N = 2-15$ ,  $d(001) = 10 \text{ \AA}$ , and  $G^2(\theta)$  for an illite unit cell.

At this point we have a fairly realistic peak shape, so let us go on and build the rest of the diffraction pattern. Figure 3.16 also shows plots of  $G^2$ . Remember,  $\Phi$  refers to the intensity of scattering from a crystallite with layers that scatter with unit intensity. A real crystal contains layers that do not have unit scattering power, but scatter with different intensities at different values of  $\theta$ . We are a big step closer to the diffraction pattern of a real crystal if we multiply  $G$  and  $\Phi$  for each value of  $\theta$ . The results of such a point-by-point multiplication are given in Fig. 3.17, which also shows a curve for an appropriate Lorentz-polarization factor, the factor for taking into account the geometric effects of the diffraction system. The profile is not very impressive because of unrealistic relative intensities, but multiplication by the Lorentz-polarization factor produces, finally, a fairly representative illite 00/ diffraction pattern (Fig. 3.18).

Ergun (1970) demonstrated that large crystals that are broken into small diffracting domains by stacking defects behave like an aggregate of crystallites whose abundances diminish exponentially with increasing thickness. Many clay minerals produce diffraction patterns whose line shapes are consistent with this model. An example has been computed for the range of  $N = 2$  to 40. The term  $q(N)$  in Eq. (3.15) was replaced by  $\exp[(2-N)/\delta]$ , a weighting coefficient, in which  $\delta$  signifies the mean defect-free distance, six unit cells for this example (Fig. 3.19).

If you closely compare Figs. 3.18 and 3.19 with the X-ray tracing of natural illite, you can see that Ergun's model has produced more realistic line shapes. In addition, in this model, the troublesome background ripples have been eliminated. More work needs to be done in applying the defect-broadening model to clay minerals, but it invariably produces the most

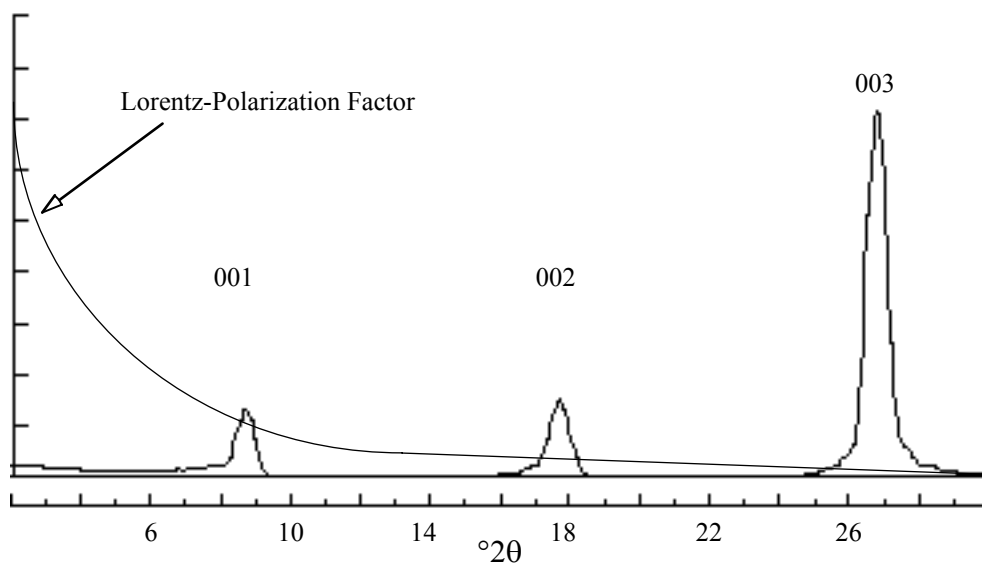


Fig. 3.17 The Lorentz-polarization factor and the product of  $G^2$  and  $\Phi$ .

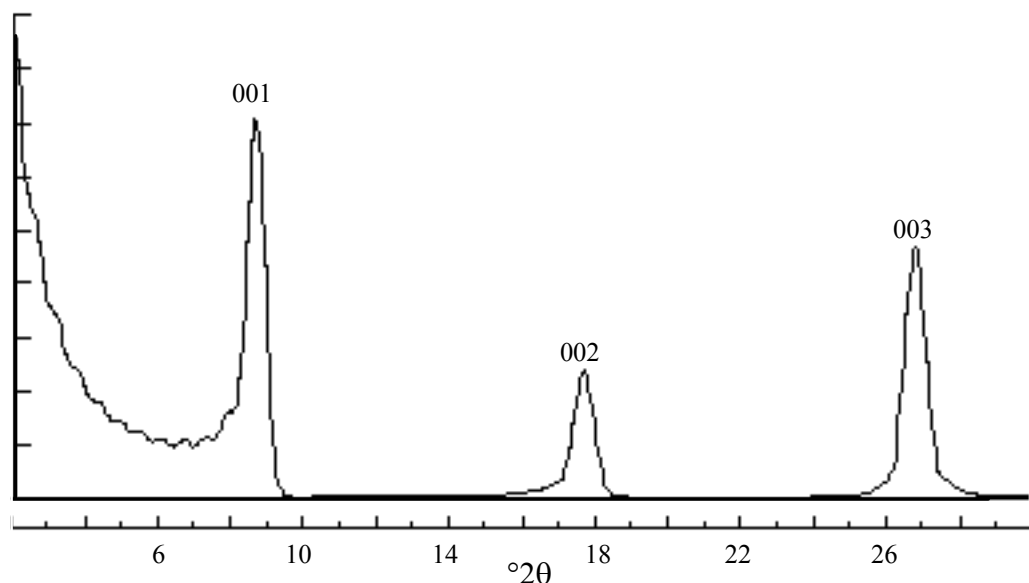


Fig. 3.18. Calculated diffraction patterns for illite,  $N=2-15$ .

realistic simulated diffraction patterns. Before leaving this subject, we need to point out that if you attempt to duplicate these calculations, your pattern will not be as realistic on the low-angle side of the 001 peak as that of Fig. 3.19. This is because NEWMOD<sup>®</sup> assumes that the surfaces of the terminal 2:1 layers of a crystallite are naked, i.e., there is no K there. This is probably realistic, but the equations developed here do not allow for this and position  $1/2K$  on the outside of each terminal 2:1 layer.

We have discussed the effects of mean  $N$  and crystallite particle-size distributions on line profile, but a complete treatment of  $00l$  line shape requires a consideration of the effects of the interplay of  $G$  and  $\Phi$  on peak symmetry. The Lorentz-polarization factor is an important component of peak intensity, but it has little or no effect on peak shape except at low diffraction angles, and we will not consider it further at present. Look at the shape of the  $G^2$  function for the illite 001 reflection (Fig. 3.16). It has low values near the high- $2\theta$  side of the illite 001 reflection and rises abruptly with diminishing  $2\theta$ . When  $G^2$  is multiplied by  $\Phi$ , the resulting peak shape is weakened on the high- $2\theta$  side and extended considerably on the low- $2\theta$  side, thus producing a marked asymmetry. By contrast,  $G^2$  is a good deal flatter through the 002 and 003 peak positions, with the result that their shapes are essentially unmodified from the form of the peak in  $\Phi$  at the 002 and 003 positions. The degree of asymmetry for a given  $00l$  reflection increases with the slope of  $G^2$  across that peak, and asymmetry increases as  $N$  diminishes because the broadest peaks are the most affected by a given slope in  $G^2$ .

For extreme cases like the illite 001 reflection, the asymmetry introduced by  $G^2$  is so great that the top of the peak is shifted toward lower  $2\theta$  values. A calculation of the profiles of various  $00l$  reflections from an illite consisting

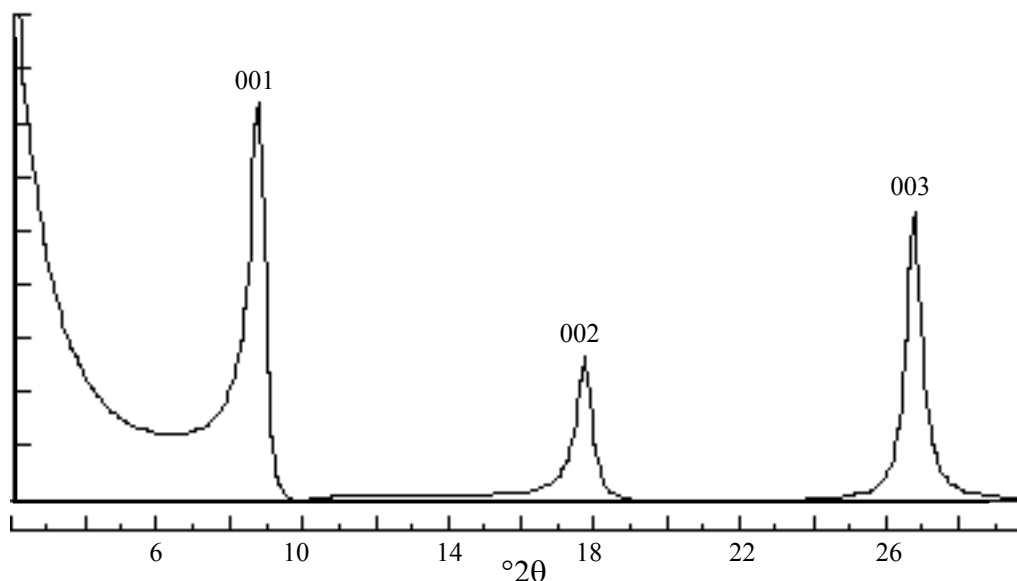


Fig. 3.19. Diffraction pattern for illite. Defect-free distance ( $\delta$ ) = 6 unit cells.

of thin crystals produces peak positions that depart from Bragg's law, and such a situation can be easily misinterpreted as evidence for interstratification with another clay mineral species.

Small crystallite or coherent domain size is often equated with poor "crystallinity." It is ironic that more information can be obtained about the structure of the unit cell from a poor crystal than from that of a good one. Extra information can be obtained because we can examine  $G$  over a small but finite range on either side of a normal Bragg peak, as we discussed in connection with Fig. 3.13. This is something that we cannot do with a large crystal because its peaks are infinitely sharp and have measurable intensities only at one point in the  $2\theta$  continuum. To be sure, the experimental patterns for large crystallites show some diffracted intensity on either side of the peak position, but remember that is caused by instrument distortion and tells us nothing about the diffraction intensity from the unit cell at angles that deviate somewhat from the ideal ones. Small crystals give information not only on the magnitude of  $G^2$  but also on the direction and magnitude of the slope of  $G^2$  in the vicinity of a peak in the interference function. W. F. Bradley (1908-1973) perceptively remarked that the interference function  $\Phi$  provides windows through which we can examine the layer transform  $G$ .

***Exercise: Calculation of the Intensity from  $d(001)$  for Illite***

To show you how the computer program simulated the diffraction tracings in the preceding section, let's calculate intensity values for diffracted beams scattered from a simplified and stylized illite unit cell. Figure 3.20 shows one unit cell layer of illite with interlayer ions of K and a fragment of the

overlying unit cell. Each layer of illite is made up of an octahedral (o) sheet sandwiched by two tetrahedral (t) sheets. The sheets are made up of planes of atoms. We have chosen to use the plane of Al and Mg in the center of the octahedral sheet as the origin for measuring distances to neighboring planes. We have listed the separation in Ångstroms starting at this plane. The number and kind of atoms in five of the planes of the illite unit cell are noted at the far right of Fig. 3.20. We will use this figure to explain the calculations associated with Table 3.1.

See that it is 10 Å from the center of the K atom at the bottom of Fig. 3.20 to the center of the K atom at the top. It is also 10 Å from the base of the lowest tetrahedral sheet to the base of the uppermost one. Is it understood that the distance from any atom in the lower unit cell to its equivalent in the upper unit cell is 10 Å? (An important way to see the geometry of this situation is to realize that there is a series of 10 Å spacings interleaved, and each will diffract at exactly the same time when the incident beam is at a Bragg angle.)

What kind of intensities will this arrangement of atoms yield? Intensity is proportional to the layer scattering factor  $G$  squared. We developed an expression for  $G$  in a preceding section (Eq. 3.9); so to calculate intensity at a chosen value of  $\theta$  we use Eq. (3.14).

In more careful work, other factors would be needed, but we need only the general idea. We will assume, for this exercise, that the  $L_p$  factor is close enough to constant for the values of  $\theta$  we use so that we may ignore it. Recall that crystallographers like to use  $F$ , the structure factor, only for specific  $hkl$  values, and therefore, for a continuous function of  $\theta$  we use  $G$ , the layer structure factor, or layer scattering factor. We will ignore a factor to allow for effects of temperature, one that allows for some of the incident radiation being absorbed, and one called the multiplicity factor that allows for differences in the relative number of a spacing of one size compared to the number of spacings of other sizes. The general power of Eq. (3.14) can be clearly demonstrated without including any of these factors. Recall how we got from Eq. (3.6), p. 78

$$F(00l) = \Re \sum_n f_n \cos \phi_n = \Re \sum_n P_n f_n \cos(2\pi l z_n / c) \quad (3.6)$$

to Eqs. 3.9 and 3.14:

$$G(\theta) = \Re \sum_n P_n f_n \cos(4\pi z_n \sin \theta / \lambda) \quad (3.9)$$

and

$$I(\theta) = [G^2(\theta)][\Phi(\theta)][L_p(\theta)] \quad (3.14)$$

From these equations, we have

$$G(\theta) = \sum_n f_n(\cos\theta_n) \quad \text{and} \quad |G(\theta)|^2 = \left[ \sum_n f_n(\cos\theta_n) \right]^2 \quad (3.16)$$

Table 3.1 shows how the parts of Eq. (3.16) are evaluated. Recall from the discussion of Fig. 3.9 that the phase angle  $\theta$  is found by assuming there is a  $360^\circ$  difference [for the (001) reflection], or one full wavelength, between the wave scattered from the lower plane of Al and Mg atoms and that scattered from the equivalent upper plane of Al and Mg atoms, i.e., the phase angle of the lower plane is  $0^\circ$  and that of the upper is  $360^\circ$ . (This is true only when the diffractometer is set at a Bragg angle, i.e., when constructive interference takes place.) Then the phase angles for waves scattered from other planes are the proportional distance of each plane times  $360^\circ$ , as we did for the phase difference for the ray scattered from atom B in Fig. 3.10. (For example, see Fig. 3.20 and Table 3.1. The plane labeled 3.4 Si's and 0.6 Al's is  $2.68 \text{ \AA}$  above the plane with 3.6 Al's and 0.4 Mg's, the plane that has been chosen as the starting point, or  $z = 0$ . Then the phase angle for the plane with 3.4 Si's and 0.6 Al's is  $2.68/10 \times 360^\circ = 96.5^\circ$ , i.e., it is  $96.5^\circ$  out of phase with the wave scattered from the Al-Mg plane. Or, another way to visualize this is to

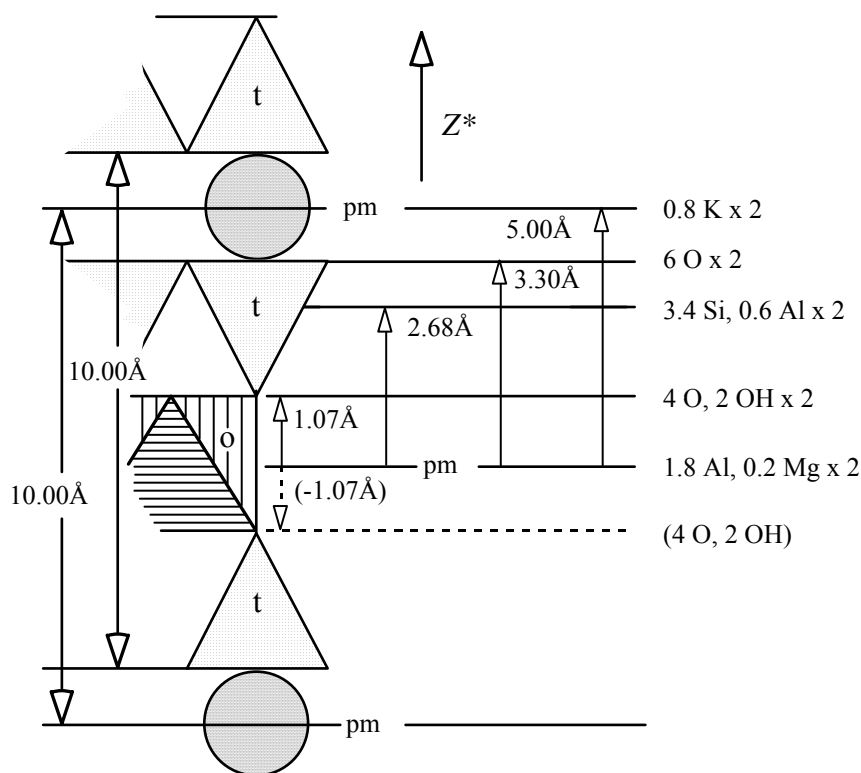


Fig. 3.20. A diagram of an edge of the illite structure showing the separation in Ångstroms of each plane of atoms above the mirror plane marked pm (because it is a pseudomirror). The contribution of each plane to the amplitude of the beam diffracted from the unit cell will be related to its fractional position in relation to the 10 Å spacing. t marks a tetrahedral sheet and o marks an octahedral sheet.

recall that at the Bragg angle for diffraction from a 10 Å spacing, 360° represents the full cycle of one sine wave. Then the 2.68 Å above the starting point is 2.68/10 of a full sine wave.)

Focus on Fig. 3.20 for a moment. See that there are three mirrors labeled pm. (These are mirrors, or pseudomirrors pm, we have invented for the sake of this description. They are not mirrors in the strict crystallographic sense.) We have given the distances between planes of atoms starting from the central atom plane in the octahedral sheet as zero. We have stopped at the mirror plane that cuts the K atom in the interlayer space of this illite crystallite. How can we do this if the unit cell dimension is 10 Å and the center of the K atom is only halfway through the 360° cycle? Do you see that the plane above the origin with 4 O's and 2 OH's is duplicated at an equal distance below a mirror plane? Correspondingly, all the planes for which we have given the atom populations are duplicated below this mirror. By the happy consequence of this mirror, the arithmetic is reduced. If you review your trigonometry, you will rediscover that  $\cos(x) = \cos(-x)$ . Starting at the origin,  $z = 0$ , the atom plane above the mirror has the coordinate 1.07 Å. There is an identical plane at the coordinate -1.07 Å. Likewise, planes of atoms are present at 2.7 and -2.7 Å, at 3.3 and -3.3 Å, and finally at 5 and -5 Å. Thus we need only consider five planes (counting the zero plane) in the cosine summation. The cosine terms for planes 2, 3, and 4 must be multiplied by 2 to account for the identical contributions of the coordinates at  $z$  and  $-z$ . You don't double the contributions of the Al and Mg plane and the K plane because they do not have mirror images above and below the center of symmetry in one unit cell. You might say that they have half an image on each side.

The column headed  $f(\theta)$  is the scattering power of the neutral atom for the Bragg angle for which the problem is being solved. Because  $f$  is a function of the Bragg angle, as well as the number of electrons of an atom, we must specify the angle for which we want the scattering power. In this case, for  $\text{CuK}\alpha$  radiation, we know that the (001) spacing of 10 Å causes diffraction at 8.8°  $2\theta$  or 4.4°  $\theta$ ; i.e., 4.4°  $\theta$  is a Bragg angle for this spacing, so we will use the scattering values for these atoms at 4.4°. Values of  $f$  are listed in tables (see Klug and Alexander, 1974, pp. 880ff). They also can be calculated by means of a simple polynomial published by Wright (1973). For  $nf(\theta)$ , simply multiply the number of atoms in the particular plane by the scattering factor, e.g., for 3.6 Al and 0.4 Mg,  $(12.1 \times 3.6) + (11.25 \times 0.4) = 48.06$ , which we've rounded off to 48.1. Notice that for the planes containing O and OH, H is ignored and only the O atoms are counted (how could this be?) The last column is then summed to find the total scattering efficiency of the unit cell ( $G$ ) of  $\text{K}_{1.6}(\text{Al}_{3.6}\text{Mg}_{0.4})(\text{Si}_{6.8}\text{Al}_{1.2})\text{O}_{20}(\text{OH})_4$  arranged as shown in Fig. 3.20. In this case it is 35.3 electron scattering units.

$G$  calculated from Eq. (3.16) will not simulate an experimental diffraction tracing.  $G$  plotted against  $2\theta$  would give the curve shown in Fig. 3.21. To get a simulation of a diffraction tracing, we must multiply  $G^2$  by the interference

Table 3.1. Evaluation of terms for Fig. 3.20 and Eq. (3.16) for a 10 Å spacing using CuK $\alpha$  radiation.

Atoms, $P_n$	$\emptyset$ (deg)	$f(\theta)$	$r^*f(\theta)$	$\cos\emptyset$	$nf(\theta)\cos\emptyset$
1.6 K	(5.00/10)(360) = 180.0	17.9	28.6	-1.000	28.6x1 = -28.6
6 O	(3.30/10)(360) = 118.8	7.6	45.6	-0.481	-21.9x2 = -43.8
3.4 Si; 0.6 Al	(2.68/10)(360) = 96.5	13.2; 12.1	52.1	-0.113	-5.9x2 = -11.8
4 O; 2 OH	(1.07/10)(360) = 38.5	7.6	45.6	0.783	35.7x2 = 71.4
3.6 Al; 0.4 Mg	(0.00/10)(360) = 0.0	12.1; 11.25	48.1	1.000	48.1x1 = <u>48.1</u>
					$G(001) = \Re = 35.3$

\* $r$  = number of atoms in plane

function  $\Phi$ , as defined in Eq. (3.10). For our sample calculation, assume the illite crystallite is 20 layers thick, each layer is 10 Å thick, and the wavelength of the CuK $\alpha$  radiation is 1.54 Å. We put these values in Eq. (3.10) as  $N = 20$ ,  $d = 10$  Å,  $\lambda = 1.54$  Å, and  $\theta = 4.4^\circ$ , as stated earlier

$$\Phi = \frac{\sin^2 [(2\pi)(20)(10 \text{ \AA})(\sin 4.4^\circ)/1.54 \text{ \AA}]}{\sin^2 [(2\pi)(10 \text{ \AA})(\sin 4.4^\circ)/1.54 \text{ \AA}]}$$

$$= \frac{\sin^2 62.57}{\sin^2 3.13}$$

[We need to introduce a qualification here and advise you that this function is very sensitive to errors when it is solved right at the Bragg angle. In fact, if you had  $\theta$ ,  $\lambda$ , and  $d$  exactly correct, the value of  $\Phi$  would be equal to  $\sin^2(n\pi)$  over  $\sin^2(\pi)$ , where  $n$  is integral and that would be indeterminate. But if you are very close, but not precisely on the Bragg position, the value of  $\Phi$  is simply equal to  $N^2$ . What allows a computer to arrive at a useful answer is that  $\pi$  is an irrational number, i.e., it is without an exact value. Play with these numbers and see for yourself. We will ignore this qualification and go on from here.]

The numbers 62.57 and 3.13 are in radians, and we know that there are  $2\pi$  radians in  $360^\circ$ , or one cycle, or one wavelength. We are interested only in how much a wave or cycle is out of phase; so we ignore all whole cycles because whole cycles will not tell us how close two waves are to being in phase. By simple arithmetic, you can find that 6.28 (i.e.,  $2 \times 3.14$ , the number of radians in one cycle) times 9 = 56.52, and  $62.57 - 56.52 = 6.05$ . Or, to say the same thing a different way, there are nine complete cycles and  $6.05/6.28$  of another in 62.57 radians. We don't need to do anything to 3.13 because it is less than one cycle. We now have a ratio of two cycles,  $6.05/3.13$ , or a

measure of phase difference. To convert these to degrees, we multiply  $360^\circ$  by the following ratios

$$(6.05/6.28)(360^\circ) = 346^\circ 49'$$

$$(3.13/6.28)(360^\circ) = 179^\circ 26'$$

The sine of  $346^\circ 49' = -0.2281$  and that of  $179^\circ 26' = 0.01$ . Now we must square these values

$$\frac{(-0.2281)^2}{(0.01)^2} = \frac{0.052}{0.0001} = 520 \text{ for } \Phi \text{ at } 4.4^\circ\theta$$

Then

$$I(001) = |G(001)|^2 [\Phi(001)][L_p(001)] = |35.3|^2 (520)[L_p(001)]$$

$$= 647,967 [L_p(001)]$$

or an intensity of 647,967 (in some arbitrary unit) times the  $L_p$  factor. [The 35.3 is the sum of  $G(001)$  taken from Table 3.1. Notice that about the same value can be read from Fig. 3.21.]

After you have followed this argument to its conclusion, solve  $\Phi$  for  $4.2^\circ$  and  $4.6^\circ \theta$ , just  $0.2^\circ$  on each side of this intense, diffracted beam (these could

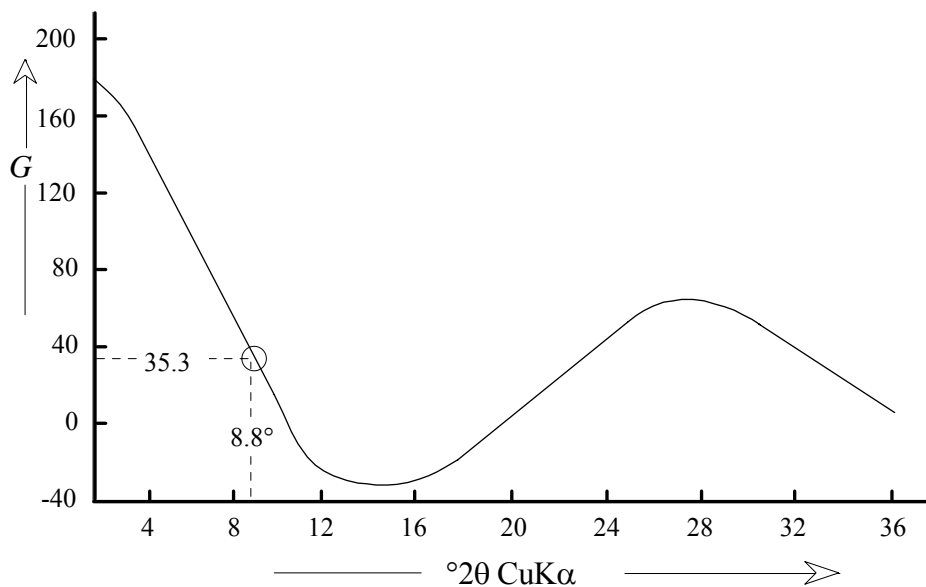


Fig. 3.21. Plot of the layer structure factor for dioctahedral illite vs.  $^\circ 2\theta$  for  $\text{CuK}\alpha$ . This does not model a diffraction tracing. We need one more step. Note that the value read from this graph is approximately the same as the  $G$  of Table 3.1.

be rays  $A'$  and  $B'$  of Fig. 3.13). Next to the main diffracted beam is precisely

where  $G$  provides useful information for small crystals. By definition  $F$  doesn't exist away from the 001 peak position.  $\Phi$ , which has a simple solution at  $4.4^\circ$ , still gives finite intensities  $0.2^\circ$  on each side of the 001 peak position. Assume that  $G$  [as in (Eq. 3.15), p. 92] stays constant over the range of the peak. Then, if you would like further insight, or just like arithmetic, you may wish to figure the intensity for the second- and third-order reflections, (002) and (003).

Are you impressed that you can calculate X-ray intensity? Do you see that this could be done for an entire diffraction tracing? This is what a computer program can do for you.

We took advantage of planes of pseudosymmetry in the illite unit cell to simplify the arithmetic. There are two reasons why this simplified approach won't work for noncentrosymmetric structures. See if you can figure them out. A note of caution. It is easy to make mistakes in assigning the correct number of atoms to the origin and to the last plane in the calculation. Look at the quantities of all the atoms you have assigned to the different atomic planes. They had better give the correct formula! (A more detailed discussion of these calculations can be found in Reynolds, 1980, pp. 255ff.)

## POINTS TO REMEMBER

To summarize:

1. The  $00l$  diffraction pattern, as a continuous function of  $\theta$ , is calculated from the expression  $I(\theta) = [G^2(\theta)][\Phi(\theta)][Lp(\theta)]$ .  $Lp$  is the Lorentz-polarization factor whose values are controlled by the geometry of the instrument and the preferred orientation of crystallites within the crystal aggregate,  $G$  is the amplitude of scattering of the unit cell in the direction  $\theta$ , and  $\Phi$  is the interference function that describes the intensity of scattering of a crystallite or mixture of crystallites, each of which contains unit layers that scatter like single electrons.
2. The breadths of  $00l$  reflections at half-height are inversely proportional to  $N$  or mean  $N$ , where  $N$  is the number of unit cells in a coherent diffracting array along the direction normal to  $d(001)$ .
3. The widths of  $00l$  peaks, in regions of  $2\theta$  where  $G^2$  is constant or nearly so, are determined by particle-thickness frequency distributions, i.e., by the relative proportions of crystallites that have different thicknesses  $N$ .
4. Peak asymmetry is caused by steep slopes of the function  $G^2$  where this function crosses a peak in the interference function  $\Phi$ . The asymmetrically extended tail of the illite 001 reflection lies in the up-slope direction of  $G^2$ , and is a good example of this. Any reflection may be displaced in the direction of increasing  $G^2$  if the slope is steep enough, or if  $N$  is small enough to produce broad peaks in the interference function, or both.

## REFERENCES

- Bragg, W. L. (1913) The diffraction of short electromagnetic waves by a crystal: *Proceeding of the Cambridge Philosophical Society* **17**, 43-57.
- Brindley, G. W., and Méring, J. (1951) Diffraction des rayons X par les structures en couches desordennees: *Acta Crystallographica* **4**, 441-47.
- Buerger, M. J. (1942) *X-Ray Crystallography*: Wiley, New York, 531 pp.
- Cullity, B. D. (1978) *Elements of X-Ray Diffraction*, 2nd ed.: Addison-Wesley, Reading, Mass., 555 pp.
- Ergun, S. (1970) X-ray scattering by very defective lattices: *Phys. Rev. B* **131**, 3371-80.
- Ewald, P. P. (1921) Das 'reziproke Gitter' in der Strukturtheorie: *Zeitschrift für Kristallographie* **56**, 129-56.
- James, R. W. (1965) *The Optical Principles of the Diffraction of X-Rays*: Vol. II, *The Crystalline State*: Series edited by Sir Lawrence Bragg, Cornell University Press, Ithaca, 664 pp.
- Klug, H. P., and Alexander, L. E. (1974) *X-Ray Diffraction Procedures*, 2nd ed.: Wiley, New York, 966 pp.
- Nadeau, P. H., Tait, J. M., McHardy, W. J., and Wilson, M. J. (1984) Interstratified X-ray diffraction characteristics of physical mixtures of elementary clay particles: *Clay Minerals* **19**, 67-76.
- Phillips, F. C. (1971) *An Introduction to Crystallography*, Fourth Edition: John Wiley & Sons, New York, 351 pp.
- Reynolds, R. C., Jr. (1976) The Lorentz factor for basal reflections from micaceous minerals in oriented powder aggregates: *Amer. Minerol.* **61**, 484-91.
- Reynolds, R. C., Jr. (1980) Interstratified clay minerals: in Brindley, G. W., and Brown, G., editors, *Crystal Structures of Clay Minerals and Their X-ray Identification*: Monograph No. 5, Mineralogical Society, London, 249-303.
- Reynolds, R. C., Jr. (1985) NEWMOD<sup>©</sup>, a Computer Program for the Calculation of Basal X-Ray Diffraction Intensities of Mixed-Layered Clays. R. C. Reynolds, Hanover, N.H. 03755.
- Reynolds, R. C., Jr. (1986) The Lorentz-polarization factor and preferred orientation in oriented clay aggregates: *Clays and Clay Minerals* **34**, 359-67.
- Reynolds, R. C., Jr. (1994) WILDFIRE<sup>©</sup>, A Computer Program for the Calculation of Three-Dimensional Powder X-Ray Diffraction Patterns for Mica Polytypes and their Disordered Variations: R. C. Reynolds, 8 Brook Rd., Hanover, N.H. 03755.
- Reynolds, R. C., Jr., and Hower, J. (1970) The nature of interlayering in mixed-layer illite-montmorillonite: *Clays and Clay Minerals* **18**, 25-36.
- Vance, E. P. (1963) *An Introduction to Modern Mathematics*: Addison-Wesley, Reading, MA, 534 pp.
- Wright, A. C. (1973) A compact representation for atomic scattering factors: *Clays and Clay Minerals* **21**, 489-90.